NTNU – Trondheim
Norwegian University of
Science and Technology

The buckling resistance of structures subjected to impulsive type actions

Andreas Landa

Marine Technology
Submission date: February 2014
Supervisor: Jørgen Amdahl, IMT

Norwegian University of Science and Technology
Department of Marine Technology

NTNU
Institutt for marin teknikk

MASTER THESIS 2013/2014

for

Stud. Techn. Andreas Landa

The buckling resistance of structures subjected to impulsive type actions

Knekkingsmotstanden til konstruksjoner utsatt for impulslaster

The present trend is to build modern structures with small weight, high slenderness and highly optimized with respect to buckling. A few examples are tethers in tension leg platforms/wind turbines, shell structures in turbine towers, substructures in new generator concepts and container vessels. During extreme actions the static buckling resistance may be exceeded for a short period. The question is whether this is critical for the structure, notably when the governing buckling modes mobilize significant inertia forces or drag forces.

Another challenge may be related to displacement controlled buckling, i.e. the end of a panel or a column is subjected to constant rate end shortening; how much is the buckling force increased by comparison with static buckling? This issue is relevant for various impact scenarios.

The purpose of the work is to study the behaviour and resistance of relevant structural components subjected to impulsive type loads, thereby developing improved insight into dynamic buckling. The work is proposed carried out in the following steps:

1. Supplement the literature review of dynamic buckling of columns, plates and shells conducted in the project work. To extent possible develop a simple algorithm in MATLAB to solve the dynamic equilibrium equations and compare with published analytic and numerical solutions.

2. Perform systematic studies of dynamic elastic buckling of simple beam-columns with varying slendernesses using USFOS. The model shall contain initial imperfections compatible with the first three buckling modes. The loading shall be either

    - Controlled rate of force increase

- Controlled rate of end shortening
- Impulsive type (sinusoidal) loading

The rate of loading/shortening or load duration shall be varied systematically. The effect of a static utilization prior to application of the dynamic force shall be investigated. The transition from one buckling mode to a higher mode when the rate of loading is increased shall be observed. The numerical results shall be compared with analytical solutions. The sensitivity to the choice of initial displacements/imperfections shall also be investigated, both with respect to total value as well as the relative composition of imperfection modes. It shall also be investigated whether a "dynamic buckling length factor" can be defined for easy buckling checks.

3. Investigate the effect of yielding on the dynamic buckling loads by running some of the analyses in pt 2 with a realistic yield strength.

4. Perform a mesh size convergence study to determine the required fineness to obtain sufficiently accurate solutions for dynamic plate buckling.

5. Perform systematic studies of dynamic elastic buckling of simply supported plates with constrained boundaries and varying slendernesses using USFOS and shell modelling. The model shall contain initial imperfections compatible with a sufficient number of buckling modes. The loading shall be either

   - Controlled rate of force increase
   - Controlled rate of end shortening
   - Impulsive type (sinusoidal) loading

   The rate of loading/shortening or load duration shall be varied systematically. The effect of a static utilization prior to application of the dynamic force load shall be investigated. The transition from one buckling mode to a higher mode when the rate of loading is increased shall be observed. The numerical results shall be compared with analytical solutions, refer e.g. Ekstrom: *Dynamic Buckling of a rectangular Orthotropic Plate*. The sensitivity to the choice of initial displacements/imperfections shall also be investigated, both with respect to total value as well as the relative composition.

6. Investigate the effect of yielding on the dynamic buckling loads by running some of the analyses in pt 5 with a realistic yield strength. Propose simple formulations for the resistance of plates to dynamic buckling.

7. If time permits perform conduct simulations of stiffened plates subjected to dynamic buckling.

8. Conclusions and recommendations for further work

For the shell element simulations it may be necessary to develop a MATLAB script to generate displaced coordinates that account for the various choices of initial deflection patterns. It is also recommended to generate scripts for the parametric simulation studies with USFOS.

Literature studies of specific topics relevant to the thesis work may be included.

The work scope may prove to be larger than initially anticipated. Subject to approval from the supervisors, topics may be deleted from the list above or reduced in extent.

In the thesis the candidate shall present his personal contribution to the resolution of problems within the scope of the thesis work.

Theories and conclusions should be based on mathematical derivations and/or logic reasoning identifying the various steps in the deduction.

The candidate should utilise the existing possibilities for obtaining relevant literature.

Thesis format

The thesis should be organised in a rational manner to give a clear exposition of results, assessments, and conclusions. The text should be brief and to the point, with a clear language. Telegraphic language should be avoided.

The thesis shall contain the following elements: A text defining the scope, preface, list of contents, summary, main body of thesis, conclusions with recommendations for further work, list of symbols and acronyms, references and (optional) appendices. All figures, tables and equations shall be numerated.

The supervisors may require that the candidate, in an early stage of the work, presents a written plan for the completion of the work. The plan should include a budget for the use of computer and laboratory resources which will be charged to the department. Overruns shall be reported to the supervisors.

The original contribution of the candidate and material taken from other sources shall be clearly defined. Work from other sources shall be properly referenced using an acknowledged referencing system.

The report shall be submitted in two copies:

- Signed by the candidate
- The text defining the scope included
- In bound volume(s)

Drawings and/or computer prints which cannot be bound should be organised in a separate folder.

The report shall also be submitted in pdf format along with essential input files for computer analysis, spreadsheets, MATLAB files etc in digital format.

Ownership

NTNU has according to the present rules the ownership of the thesis. Any use of the thesis has to be approved by NTNU (or external partner when this applies). The department has the right to use the thesis as if the work was carried out by a NTNU employee, if nothing else has been agreed in advance.

Thesis supervisors

Prof. Jørgen Amdahl

Contact person at Aker Solutions: Tore Holmås

Deadline: February 24, 2014

Trondheim, August 26, 2013

Jørgen Amdahl

Preface

This report is a result of a master thesis conducted at the Department of Marine technology at the Norwegian University of Science and Technology. The thesis deals with the buckling resistance of structures subjected to impulsive type actions.

I would like thank Professor Jørgen Amdahl for his guidance and help during the work period. I am also grateful to Martin Storheim and Ekaterina Kim for their contributions.

Andreas Landa

Trondheim, february 2014

Scope of work

The main focus in this thesis is to investigate different parameters connected to dynamic buckling on columns and plates. These parameters are:

- Reduced slenderness
- Loading rate
- Transition from one buckling mode to a higher mode when the rate of loading is increased
- Sensitivity to choice of initial imperfections, both with respect to total value as well as the relative composition
- Use of realistic value for yield strength

The objective is to identify the different parameters influence on dynamic buckling loads and buckling modes. This is done by studying published theory on the subject dynamic buckling. Analysis on beam-columns and plates are also performed to increase the insight in the phenomena dynamic buckling.

Summary

The behavior and resistance of structural components subjected to impulsive type loads is investigated. An increased insight into dynamic buckling is achieved by performing a literature study, together with analyses on beam-columns and plates. The analyses are done in the programs *USFOS* and *ABAQUS*.

The literature study defines two forms of dynamic buckling; *vibration buckling* and *pulse buckling*. The thesis' main focus is on dynamic buckling of beam-columns and plates. This can be related to slamming loads on ships or collisions between ships and offshore rigs. To be able to describe dynamic buckling properly, a theoretic foundation is created. The basic equations established by (Lindberg and Florence, 1987) are derived, as well as a mathematical description of dynamic buckling. The derivation show some of the basic features of pulse buckling for an axially loaded bar.

Different parameters effect on dynamic buckling loads are also investigated. These parameters are load duration, shape and magnitude of initial imperfections, material choice and reduced slenderness. The parameters effect on the dynamic loading factor is also included in the study. It is shown that the dynamic loading factor may drop below unity for loading durations close to the natural period of the component. The parameters effect on the buckling loads is shown to be significant, and is therefore further investigated in the analysis.

An axially loaded beam-column is analyzed in *USFOS*. Steel is the material of choice. The beam-column contains initial geometrical imperfections compatible with the three first buckling modes. By varying the loading rate, the transition from one buckling mode to a higher mode is investigated. The effect of changing the magnitude of imperfections is also considered, as well as the composition of the imperfections. The reduced slenderness of the beam-column is varied, and it is found that the effect of this change on dynamic buckling loads is significant. To investigate the beam-columns behavior in real life, there are performed analyses with using a realistic value for the yield strength.

A plate loaded with an edge load is analyzed in *ABAQUS*. The plate's eigenmodes are found by performing an eigenvalue analysis. The eigenvalues are implemented as initial imperfections. The effect of using different combinations and scaling of the eigenmodes are investigated by considering the change in the dynamic buckling loads. The effect of varying the reduced slenderness is also found, and by varying the loading rate the transition from one buckling mode to a higher mode is investigated. It is found that parameters such as reduced slenderness and scaling of the imperfections have a major influence on the dynamic buckling load. To verify the results from the analysis performed in *ABAQUS*, analytical results are obtained from (Ekstrom, 1973) and by using *MATLAB*.

Sammendrag

Knekkingsmotstanden til konstruksjoner utsatt for impulslaster er undersøkt i denne oppgaven. Et litteraturstudium er sammen med analyser gjennomført for å øke innsikten til fenomenet *dynamisk knekking*. Bjelker og plater er hovedfokuset. Analysene er gjennomført i programmene *USFOS* og *ABAQUS.*

I litteraturstudiet defineres to typer dynamisk knekking; *vibrasjonsknekking* og *knekking grunnet pulslaster*. Dynamisk knekking av bjelker og plater kan for eksempel inntreffe i skrogkonstruksjonen til et skip grunnet høye bølgelaster, eller i forbindelse med kollisjoner mellom skip og oljeplattformer. For å kunne beskrive dette på en god måte, blir et teoretisk grunnlag etablert ved utledning av ligningene utarbeidet av (Lindberg and Florence, 1987). Utledningen viser noen av de grunnleggende egenskapene for dynamisk knekking av en aksielt belastet stav.

Forskjellige parameteres effekt på dynamisk knekklast er også undersøkt. Eksempler på parametere er; lastperiode, form og størrelse på geometriske imperfeksjoner, materialvalg og redusert slankhet. Den dynamiske lastfaktoren er også inkludert i analysen. Det er vist at den dynamiske lastfaktoren kan være mindre enn 1 hvis lastperioden er i nærheten av komponentens egenperiode. Dette vil føre til at den dynamiske knekklasten blir mindre enn den statiske knekklasten. Parameterne undersøkt viser seg å ha stor innflytelse på den dynamiske knekklasten, og er derfor grundig analysert i oppgaven.

En aksielt lastet bjelke av stål er analysert i *USFOS*. Bjelken er modellert med geometriske imperfeksjoner opp til tredje grad. Ved å variere hastigheten på den aksielle lasten er overgangen mellom de forskjellige knekkformene bestemt. Størrelsen på imperfeksjonene viser seg også å ha innvirkning på knekklasten, det samme med bjelkens reduserte slankhet. For å kunne relatere analysene til virkeligheten, er analyser ved bruk av realistisk flytspenning også gjennomført.

En plate belastet av en lateral last er analysert i *ABAQUS*. Platens egenmoder er funnet ved en egenverdianalyse. Egenmodene er implementert som geometriske imperfeksjoner. Som for bjelken, blir forskjellige kombinasjoner og størrelser på egenmodene undersøkt ved å betrakte endringene i dynamisk knekklast. Overgangen mellom de forskjellige egenmodene blir etablert ved å variere hastigheten av den innkommende lasten. Effekten av å variere platens slankhet blir også undersøkt. Det viser seg at kombinasjonen av endringer i både valg av egenmoder og platens slankhet har stor innvirkning på den dynamiske knekklasten.

For å verifisere resultatene blir en analytisk løsning funnet fra (Ekstrom, 1973). Ved å bruke *MATLAB* blir arbeidet fra (Ekstrom, 1973) sammenlignet med resultater med *ABAQUS*.

Content

List of figures

List of tables

Nomenclature

A	=	Area, [m^2]
A_n, a_n	=	Fourier coefficients
a,b,t	=	Dimensions of plate, [m]
C	=	Stress wave velocity, [m/s]
c	=	Loading rate, [N/m^2s]
D_x, D_y, D_1, D_{xy}	=	Flexural rigidities, [Nm]
dx	=	Incremental length in x-direction, [m]
E	=	Young's modulus, [MPa]
EI	=	Flexural stiffness, [Nm^2]
I	=	Moment of inertia, [m^4]
L	=	Length of bar, [m]
l_k	=	Buckling length, [m]
M	=	Moment, [Nm]
m	=	Number of half-waves in buckling mode, [-]
P	=	Axial load, [N]
$(P_{cr})_s$	=	Static buckling load, [N]
$(P_{cr})_d$	=	Dynamic buckling load, [N]
p	=	Compressive stress, [MPa]
p_1	=	Static critical stress, [MPa]
Q	=	Shear force, [N]
$R(\lambda,\tau)$	=	Scalar measure of response
q(x,t)	=	Loading histories
q_n	=	Solution-coefficient
S	=	Dynamic similarity number, [-]

T	=	Period, [s]
T_b	=	Period of first free lateral vibration, [s]
t_0	=	Load duration, [s]
v	=	Velocity of impacting load, [m/s]
w_0	=	Initial imperfection in normal direction, [m]
y_0	=	Initial displacement, [m]
α	=	Buckling load amplification coefficient, [-]
β, λ	=	Reduced slenderness, [-]
γ	=	Specific weight, [N/m^3]
ε_{cr}	=	Critical strain, [-]
ς_0	=	Non-dimensional initial deflection, [-]
ς	=	Non-dimensional total deflection, [-]
η_{cr}, η_p	=	Preferred mode of buckling, [-]
ρ	=	Material density, [kg/m^3]
σ_Y	=	Yield stress, [MPa]
σ_E	=	Euler stress, [MPa]
τ	=	Non-dimensional time, [-]
ν, ν_{xy}, ν_{yx}	=	Poissons ratio, [-]

Acronyms

DLF	=	Dynamic loading factor

1 Introduction

The development of structures with small weight, high slenderness and highly optimized with respect to buckling, has led to increased focus on the topic dynamic buckling. The importance of studying the dynamic stability of such structures is crucial to ensure the required level of safety in design. Examples of structures that are vulnerable to dynamic buckling are tethers in tension leg platforms, shell structures in turbine towers and landing gear of airplanes.

The difference between static buckling and dynamic buckling is the duration and type of loading. During dynamic buckling the loading is time dependent, and the dynamic buckling load may exceed the static buckling load. This happens over a short period of time, and the question is whether this is crucial for the structure. It is commonly recognized that under short loading durations a structure may withstand dynamic buckling which are in excess of its static bifurcation load(Weller et al., 1989).

According to the dynamic loading characteristics, the studies can be divided into three categories, buckling under high impact velocity, buckling under low impact velocity, and buckling under intermediate impact velocity(Ma et al., 2006). In this thesis' field of interest, marine technology, intermediate impact velocity is of most interest. One example of such a load is fluid-solid slamming. This can happen when a ship is slammed by sea waves. In this case one has to investigate the slamming loads influence on the beams and plates in the ship structure. Other examples are when an offshore rig is subjected to sea waves. Here, the structural members are under intermediate velocity fluid-solid impact (Cui et al., 1999). The focus on structures subjected to dynamic buckling started as early as in the 1940-1950s. (Pian and Siddal, 1950) concluded after a thorough investigation of a strut under eccentric axial loading of an impact type, that a load much greater than the *Euler* load could be applied to a strut if the period of application were much less than the first natural period of the strut.

Several factors will have influence on the dynamic buckling load. It is shown that initial geometrical imperfection, duration of impulse and effective slenderness have a major influence on the buckling loads whereas the effect of material is secondary(Ari-Gur et al., 1982).

The problem when dealing with dynamic buckling is the limited amount of publications. Over the recent years the focus on the topic has increased, due to the trend to build slender structures which are sensitive to dynamic buckling. Due to this development it is expected that dynamic buckling will be an important aspect to consider for designers of offshore structures in the future.

2 Theory

When dealing with dynamic buckling, structures subjected to dynamic loads are considered. It is important to differ between buckling from oscillatory loads, and buckling from transient loads consisting of a single pulse characterized by its amplitude, shape and duration. The first type is called *vibration buckling* and the latter is called *pulse buckling*. The term pulse is used because it tends to emphasize the high amplitude and short duration. This force amplitude is often much higher than the static load(Lindberg and Florence, 1987). The two forms of dynamic buckling are described in figure (2.1). Figure (2.1a) shows vibration buckling where the bar oscillates at a frequency twice the size of the lowest bending frequency of the unloaded bar. It is called vibration buckling due to the similarity to resonant vibrations. Figure (2.1b) shows pulse buckling with the corresponding force/time graph showing the pulse force. Pulse buckling will be this thesis' main focus.

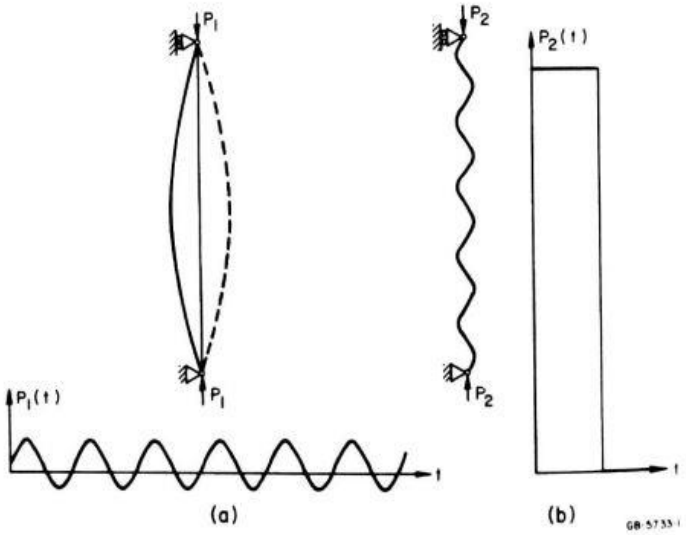

Figure 2.1: Vibration buckling & pulse buckling

Dynamic buckling can be divided into three categories, buckling under low impact velocity, buckling under high impact velocity and buckling under intermediate impact velocity (Ma et al., 2006). Structural elements which are subjected to dynamic buckling are bars, plates, rings and shells (Lindberg and Florence, 1987).

(Budiansky and Hutchinson, 1964) established a criteria for dynamic buckling. Consider a structure with a group of loading histories $q(\vec{x},t)$, generated by varying λ in equation(2.1).

$$q(\vec{x},t) = \lambda q_0(\vec{x},t) \tag{2.1}$$

Assume that $t \geq 0$ and is $q_0(\vec{x},t)$ a particular function of position x and time t, while λ is a scalar parameter. A critical value of λ can be defined for dynamic buckling. The next step is to set up a significant scalar measure of the response of the structure to $q(\vec{x},t)$, e.g. stress, deflection etc. This scalar is called $R(\lambda,t)$. Further, equation (2.2) defines the following.

$$R_{\max}(\lambda,T) = \max_{0\leq t\leq T}\left[R(\lambda,t)\right] \tag{2.2}$$

In equation(2.2), T is the largest value of t that is of interest. To find the criteria for dynamic buckling a plot of $R_{\max}(\lambda,T)$ versus λ is considered, see figure (2.2). From figure (2.2) it can be seen that R_{max} rises very steeply over a narrow range of λ. The critical value for dynamic buckling, λ_D, is defined to be the value of λ in the middle of this range. This criterion for buckling was proposed by (Budiansky and Hutchinson, 1964).

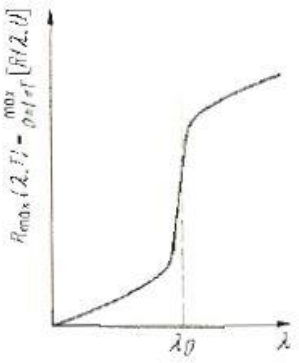

Figure 2.2: Buckling criterion

When a column is subjected to axial impact, the column will experience an axial stress wave propagation. In most studies, this effect is disregarded by assuming that the strain distribution along the column length is uniform after the impact. This situation will however, occur at a later time after the initiation of impact (Ji and Waas, 2013).

Figure (2.3) shows a number of photographs of a long column which is impacted at one end, i.e. pulse buckling. The figure shows how the axial compression wave propagates as the time increases. From the figure it is seen that the buckling is concentrated near the impacted end because the axial load is experienced for the longest time at this location. During pulse buckling it is observed that a band of preferred modes grows more rapidly than others. This is

another feature that extinguishes pulse buckling from vibration buckling. The buckling modes in pulse buckling depends on the load and must be determined as a part of the solution(Lindberg, 2003).

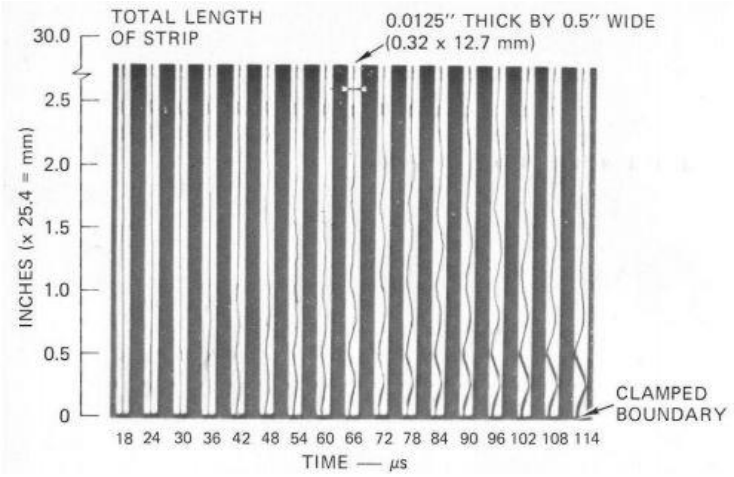

Figure 2.3: Pulse buckling

2.1 Structures subjected to dynamic buckling

Within marine technology there are several structures that are vulnerable to dynamic buckling. Due to the sea environment, the interaction between waves and the structure are most relevant. The corresponding dynamic load is fluid-solid slamming(Cui et al., 1999). On a ship, the beams and plates on the deck are subjected to buckling under intermediate velocity. A container ship has large bow flares to be able to transport as many containers as possible. This will lead to large slamming loads, and dynamic buckling can occur.

Other examples of structures that experience buckling under intermediate velocity are landing gear on an airplane during landing, offshore rigs and wind turbine towers. For offshore structures collisions plays an important role when dealing with dynamic buckling. One example is a collision between a supply vessel and the leg of a platform. This can be related to displacement controlled buckling, i.e. the end of a panel or a column is subjected to constant end shortening. The knowledge of dynamic buckling in design is limited and it is often based on the use of a static buckling load to which a load factor is applied. It is therefore essential that this factor is correct, a wrong value will lead to overdesigned structures or in worst case, catastrophic failure (Featherston et al., 2010).

2.2 Equation of motion

The derivation of the equation of motion was performed by (Lindberg and Florence, 1987). A simply supported uniform bar under axial compression is considered. Elastic buckling is assumed for the bar with length L and compressive force P, see figure (2.4).

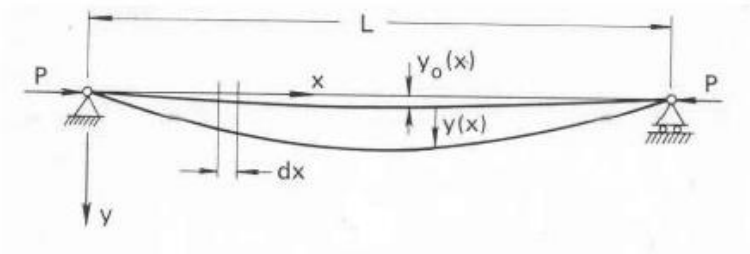

Figure 2.4: Simply supported uniform bar

The equation of motion is found by considering dynamic equilibrium of an incremental length *dx* of the element, see figure (2.5).

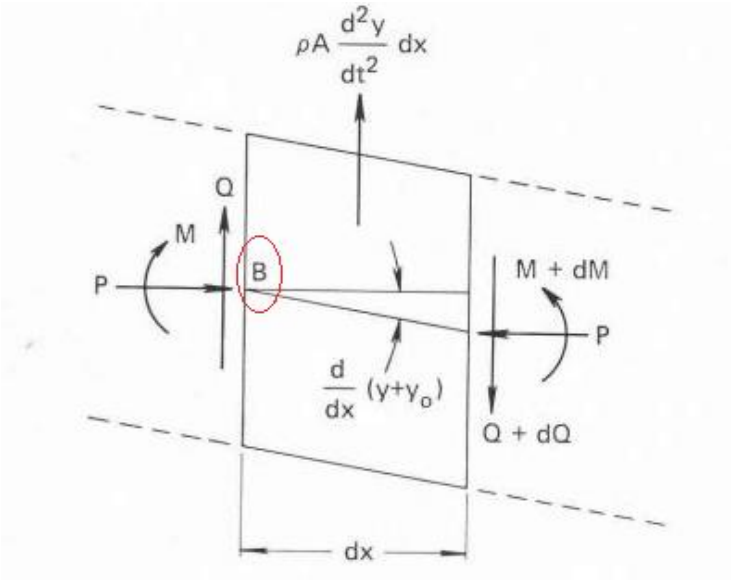

Figure 2.5: Incremental length of element

The positive direction is taken as the direction of the moment and shear force in figure (2.5). When considering the equilibrium in y-direction, the following is obtained:

$$-Q - \rho A \frac{\partial^2 y}{\partial t^2} dx + (Q + dQ) = 0 \qquad (2.3)$$

The term $\rho A \frac{\partial^2 y}{\partial t^2} dx$ is the inertia force acting on the element. Equation (2.4) is obtained when rearranging equation(2.3).

$$\rho A \frac{\partial^2 y}{\partial t^2} = \frac{dQ}{dx} \tag{2.4}$$

Taking the sum of moments about point *B* in figure (2.5), and neglecting rotary inertia of the element, gives:

$$M - \rho A \frac{\partial^2 y}{\partial t^2} dx \frac{dx}{2} + (Q + dQ)dx - (M + dM) + P \frac{\partial}{\partial x}(y + y_0)dx = 0 \tag{2.5}$$

The initial displacement is accounted for by adding the term y_0 to equation (2.5). Second order terms are neglected giving equation (2.6).

$$Q = \frac{\partial M}{\partial x} - P \frac{\partial}{\partial x}(y + y_0) \tag{2.6}$$

The relation between the curvature of the bar axis and the bending moment, is found by neglecting the effects of shear deformations and shortening of the bar axis, see equation (2.7).

$$EI \frac{\partial^2 y}{\partial x^2} = -M \tag{2.7}$$

The differential equation for the bar is found by differentiating (2.6), and eliminating Q by using (2.4), and M by (2.7) differentiating twice. This will give the equation of motion, equation (2.8).

$$EI \frac{\partial^4 y}{\partial x^4} + P \frac{\partial^2}{\partial x^2}(y + y_0) + \rho A \frac{\partial^2 y}{\partial t^2} = 0 \tag{2.8}$$

2.3 Analytical solution for dynamic buckling

The analytical solution for the dynamic buckling problem was performed by (Lindberg and Florence, 1987). When equation (2.8) is established, it is possible to obtain an analytical solution for dynamic buckling. To keep the theory simple, the material behavior of the bar is assumed to be rigid, linear-plastic hardening (Ma et al., 2006). As previously mentioned dynamic buckling is different from static buckling. In dynamic buckling loads in excess of the static buckling load is experienced over shorter periods of time. Because of this feature in the dynamic problem, rather than seeking the maximum load that can be carried, we specify a load and seek the response (Lindberg, 2003). The same bar as in figure (2.4) is considered.

The magnitude of the load P can be much larger than in the case of static buckling. In static buckling the buckling load is known as the *Euler load.* The differential equation (2.8) governs the motion of the bar. This equation is divided by EI and the following parameters are introduced

$$k^2 = \frac{P}{EI}, r^2 = \frac{I}{A}, c^2 = \frac{E}{\rho} \tag{2.9}$$

The parameters introduced in equation (2.9) are used in equation (2.8).

$$\frac{\partial^4 y}{\partial x^4} + k^2 \frac{\partial^2 y}{\partial x^2} + \frac{1}{r^2 c^2} \frac{\partial^2 y}{\partial t^2} = -k^2 \frac{\partial^2 y_0}{\partial x^2} \tag{2.10}$$

To be able to continue the derivation boundary conditions have to be introduced. Zero moment and displacement at the end of the bar is assumed. These conditions will give

$$y = \frac{\partial^2 y}{\partial x^2} = 0, at\ x = 0\ and\ x = L \tag{2.11}$$

The solution of equation (2.10) by using the boundary conditions given in (2.11), can be expressed by a Fourier sine series in x, hence a product solution is taken

$$y(x,t) = \sum_{n=1}^{\infty} q_n(t) \sin \frac{n\pi x}{L} \tag{2.12}$$

A product solution can also be assumed for the initial displacement $y_0(x)$

$$y_0(x) = \sum_{n=1}^{\infty} A_n \sin \frac{n\pi x}{L} \tag{2.13}$$

The coefficient A_n can be found from

$$A_n = \frac{2}{L} \int_0^L y_0(x) \sin \frac{n\pi x}{L} \tag{2.14}$$

It is now possible to substitute equation (2.12) and (2.13) into equation (2.10), to give the equation of motion for the Fourier coefficients $q_n(t)$

$$\left[\frac{n^4 \pi^4}{L^4} - k^2 \frac{n^2 \pi^2}{L^2} \right] q_n + \frac{1}{r^2 c^2} \ddot{q}_n = k^2 \frac{n^2 \pi^2}{L^2} A_n \tag{2.15}$$

With some rearranging the more standard from is obtained

$$\ddot{q}_n + \frac{r^2 c^2 n^2 \pi^2}{L^2}\left[\frac{n^2\pi^2}{L^2} - k^2\right] q_n = r^2 c^2 k^2 \cdot \frac{n^2\pi^2}{L^2} A_n \tag{2.16}$$

The sign of the coefficient q_n decides the nature of the solutions, i.e. whether the solutions are hyperbolic or trigonometric. If $n\pi / L < k$ the coefficient is negative and the solutions are hyperbolic, and if $n\pi / L > k$ the coefficient is positive and the solutions are trigonometric. The definition of *k* is found in equation (2.9). From this it is seen that the mode numbers *n*, determines the solution. Thus, if the mode numbers are large enough, i.e., $n > kL/\pi$, the displacements are trigonometric. This means that the displacements are bounded and no significant displacement change accompanies the initial imperfections. Over the lower range of mode numbers, $n < kL/\pi$, the hyperbolic solutions grow exponentially with time and have the potential of greatly amplifying small initial imperfections. These modes are therefore called *buckling modes (*Lindberg and Florence, 1987).

The relationship with the static buckling problem can be seen by considering the mode number that separates the trigonometric and hyperbolic solutions, i.e. $n = kL/\pi$. This mode number will give a wavelength corresponding to the wavelength of static buckling under the load *P*. Another way to see the relationship with the static buckling problem is to analyze the deflection shape. From equation (2.12) it is seen that the deflection shape of the bar is a sine wave with *n* half-waves. For $n = kL/\pi$ this shape is given by *sin kx*. If one half-wave of this shape is considered, this will correspond to the buckling mode of a simple pinned Euler column. This shape will occupy a distance given by

$$kx_{st} = \pi \tag{2.17}$$

or

$$x_{st} = \frac{\pi}{k} \tag{2.18}$$

k is recognized from equation (2.9), and the following is obtained

$$P = \frac{\pi^2 EI}{x_{st}} \tag{2.19}$$

Equation (2.19) is known as the static buckling load of an Euler column of length x_{st} under load *P*. (Lindberg, 2003) proposed a statement that any load greater than $P_1 = \pi^2 EI / L$, not just the eigenvalues of the static problem, gives unstable motion. This can also be seen from equation (2.16), when the coefficient q_n is negative, or if

$$\frac{n^2\pi^2}{L^2} - k^2 < 0 \tag{2.20}$$

It is seen from (2.20) that the expression is most negative for $n = 1$, since $k^2 = EI / L$ is positive. When $n = 1$ the motion will be unstable, which is also often the case for dynamic problems. In dynamic problems, the load is in excess of the Euler load, i.e. $P >> \pi^2 EI / L^2$. The mode numbers will therefore be high and the wavelengths so short that the total length of the bar becomes unimportant. A case of dynamic buckling is a bar impacted at one end, and due to the finite speed of the axial wave propagation, buckling occurs before any signal is received from the opposite end. Hence, the total length of the bar has no significance at all, and another characteristic length other than the length of the bar is wanted. The nature of the motion changes at the static Euler wavelength, $x_{st} = \pi / k$, and therefore $1/k$ can be used as the characteristic length in x-direction. This can also be done in the lateral direction. The lateral deflections can be normalized with respect to the radius of gyration r of the cross section. The ratio of these lengths is a significant parameter and can be denoted by s.

$$s^2 = r^2 k^2 = \frac{r^2 P}{EI} = \frac{P}{AE} = \varepsilon \tag{2.21}$$

The following variables are introduced to be able to include these lengths into the equation of motion

$$w = \frac{y}{r} \qquad \xi = kx = \frac{sx}{r} \qquad \tau = \frac{s^2 ct}{r} \tag{2.22}$$

When equation (2.22) is introduced the equation of motion (2.8) becomes

$$w'''' + w'' + \ddot{w} = w_0'' \tag{2.23}$$

The primes in equation (2.23) indicate differentiation with respect to ξ, while the dots indicate differentiation with respect to τ. The boundary conditions presented by equation (2.11) become

$$w = w'' = 0 \quad at\ \xi = 0 \quad and \quad \xi = l = \frac{sL}{r} \tag{2.24}$$

The product form of the solution becomes

$$w(\xi, \tau) = \sum_{n=1}^{\infty} g_n(\tau) \sin \frac{n\pi\xi}{l} \tag{2.25}$$

Similarly, the initial displacement is written according to equation (2.26).

$$w_0(\xi) = \sum_{n=1}^{\infty} a_n \sin\frac{n\pi\xi}{l} \tag{2.26}$$

where

$$a_n = \frac{2}{l}\int_0^l w_0(\xi)\sin\frac{n\pi\xi}{l}d\xi \tag{2.27}$$

If a wave number η is introduced, defined as $\eta = n\pi / l$, the equations of motion for the Fourier coefficients $g_n(\tau)$ can be derived as follows

$$\ddot{g}_n + \eta^2(\eta^2 - 1)g_n = \eta^2 a_n \tag{2.28}$$

Equation (2.28) will correspond to equation (2.16), and in the new notation the transition from hyperbolic to trigonometric solutions occur at $\eta = 1$. The general solution to equation (2.28) is

$$g_n(\tau) = C_n \cosh p_n\tau + D_n \sinh p_n\tau - \frac{a_n}{1-\eta^2} \quad for \quad \eta < 1 \tag{2.29}$$

$$g_n(\tau) = C_n \cos p_n\tau + D_n \sin p_n\tau - \frac{a_n}{1-\eta^2} \quad for \quad \eta > 1 \tag{2.30}$$

where

$$p_n = \eta\left|1-\eta^2\right|^{1/2} \tag{2.31}$$

If equation (2.29) and (2.30) is introduced in (2.25), the general solution for the lateral displacement is obtained

$$\begin{aligned} w(\xi,\tau) = &\sum_{n=1}^{N}\left[C_n \cosh p_n\tau + D_n \sinh p_n\tau - \frac{a_n}{1-\eta^2}\right]\sin\frac{n\pi\xi}{l} \\ &+ \sum_{n=N+1}^{\infty}\left[C_n \cos p_n\tau + D_n \sin p_n\tau - \frac{a_n}{1-\eta^2}\right]\sin\frac{n\pi\xi}{l} \end{aligned} \tag{2.32}$$

Since *w* is measured from the initial displacement w_0, the initial conditions are

$$w(\xi,0) = \dot{w}(\xi,0) = 0 \tag{2.33}$$

If equation (2.33) is applied to (2.32), the final solution is found. Equation (2.34) shows qualitatively the exponential growth of the buckling terms.

$$w(\xi,\tau)=\sum_{n=1}^{\infty}\frac{a_n}{1-\eta^2}\begin{bmatrix}\cosh p_n\tau-1\\ \cos p_n\tau-1\end{bmatrix}\sin\frac{n\pi\xi}{l} \tag{2.34}$$

The hyperbolic form is taken for $\eta<1$, while the trigonometric form is taken for $\eta>1$. As previously mentioned small initial imperfections can be greatly amplified under the hyperbolic form, hence this is the form of interest when dealing with the buckling problem. As the time increases the wave number of the most amplified mode can be determined. The wave number of the most amplified mode is obtained approximately as $\eta_{cr}=0.707$. This number is found by differentiating the *amplification function* for $\eta<1$. The *amplification function* is the ratio between the Fourier coefficients a_n of the initial displacements and the coefficients $g_n(\tau)$ as the structure buckles(Lindberg and Florence, 1987). In this case this function is given by equation (2.35).

$$G_n(\tau)=\frac{g_n(\tau)}{a_n}=\begin{Bmatrix}\dfrac{1}{1-\eta^2}\begin{bmatrix}\cosh p_n\tau-1\\ \cos p_n\tau-1\end{bmatrix} & if \quad \eta\neq 1\\ \tau^2/2 & if \quad \eta=1\end{Bmatrix} \tag{2.35}$$

The *amplification function* can be plotted to get a better insight in how the parameter τ affects the imperfection amplification, see figure (2.6) taken from (Lindberg, 2003). In the figure, η is treated as a continuous variable, and τ is the dimensionless time that spans from significant amplification occurring for a range of both trigonometric and hyperbolic modes. A first-order criterion for critical loads at the onset of pulse buckling has been found by experiments to occur at $\tau=8$. The experiments showed that nonlinear effects, such as onset of plastic hinges began at this value for τ. For a given structure, specification of τ = 8 can be used to calculate combinations of load amplitude and duration that cause buckling. In fact, from the definitions of *s* and τ in equation (2.21) and (2.22), τ is proportional to the applied impulse (Lindberg, 2003).

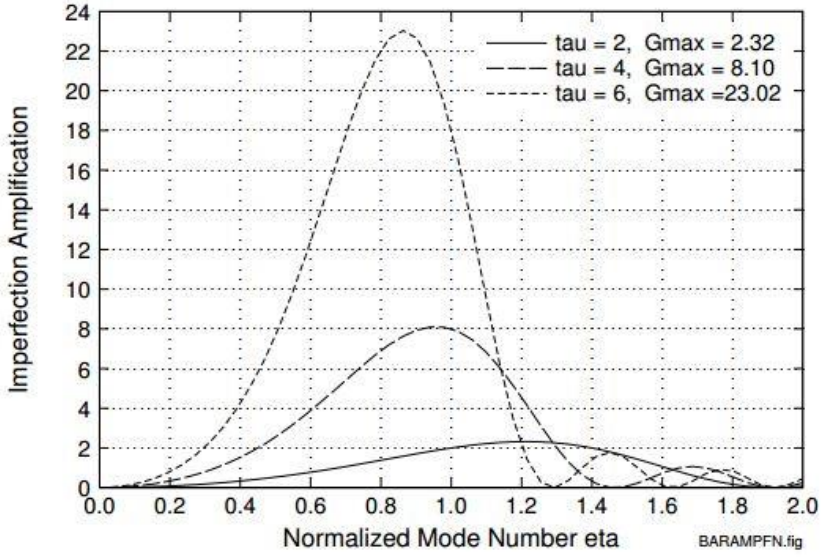

Figure 2.6: Amplification function

The approximation of $\eta_{cr} = 0.707$ can be used in the definition of p_n stated in equation (2.31). A better estimate of η_{cr} will then be

$$\eta_{cr} \approx \frac{1}{\sqrt{2}} \cdot \sqrt{\frac{\tau}{\tau - 2}} \tag{2.36}$$

By calculating η_{cr} for different values of τ it is found that a rough estimate of the wave number of the most amplified mode can be taken as simply $\eta_{cr} \approx \eta_p \equiv 0.8$. This is called the *preferred mode of buckling.*

The above derivation has shown some basic features of the bar pulse buckling, for an axially loaded bar. The effect of boundary conditions and load category on the dynamic beam buckling under transverse load is still not understood completely. Analytical solutions of the pulse buckling problems are very complicated. Numerical simulations can therefore play an important role to identify the dynamic instability critical load for various load conditions(Ma et al., 2006). By using the analysis tool *LS-DYNA*, (Ma et al., 2006) performed numerical simulations to find the dynamic response of a uniform beam model. The beam was loaded transversely with a pulse load, and it was found that the results agreed with the dynamic plastic-flow buckling theory developed for axially loaded bars showed above, and originally performed by (Lindberg and Florence, 1987). The results from (Ma et al., 2006) agreed with the dynamic plastic-flow theory developed for axially loaded bars (Lindberg and Florence, 1987) that the vibration modes corresponding to $\eta > 1$ are bounded and the displacements of

the corresponding modes is not significantly amplified with the initial imperfections. This is shown in figure (2.7).

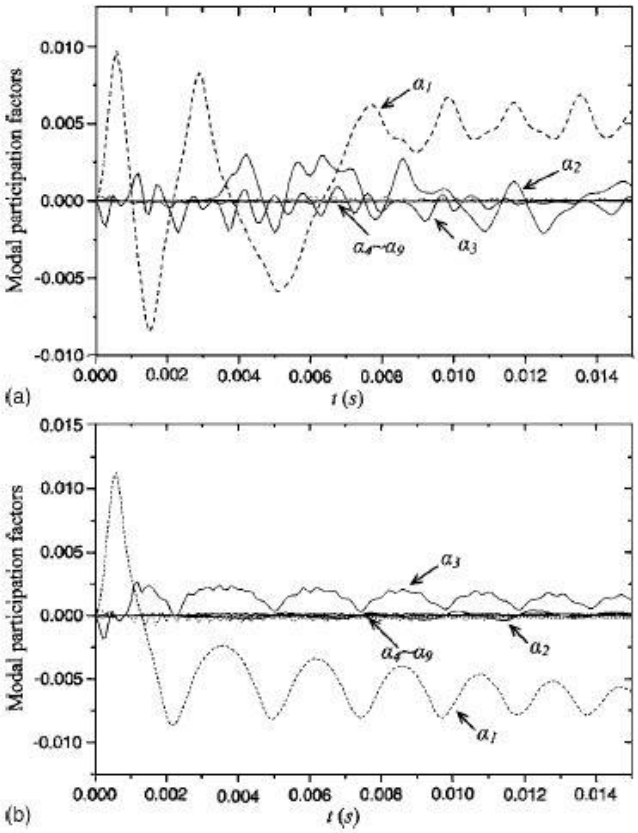

Figure 2.7: Time history of modal participation factors: P = (a) 1200N (b) 1550N

From figure (2.7) it is observed that the beam response is approximately dominated by the three first modal participation factors (α_1, α_2, α_3) and modes shaped because the other modal participation factors are relatively small.

2.4 Different parameters effect on dynamic buckling

When dealing with dynamic buckling there are many parameters to take into account. Since dynamic buckling is time-dependent, it is of interest to investigate the effect of duration of the loading. Other parameters worth investigating are initial imperfections, reduced slenderness, dynamic loading factor and material choice.

2.4.1 Effect of duration of loading

The duration of loading is an important factor to consider when dealing with dynamic buckling. As previously mentioned, the time-dependence distinguishes dynamic buckling from static buckling. It is important to have knowledge about the duration of the loading to be

able to compare it to the systems eigenvalues. The reason for this is that in cases where load durations is close to the first natural period of lateral vibrations, the *dynamic buckling* load of a plate might be smaller than the classical characteristic bifurcation load for a corresponding perfect structure(Weller et al., 1989).

(Weller et al., 1989) performed a study where dynamic buckling of beams and plates subjected to axial impact was investigated. The duration of loading was one of many parameters analyzed closely. The specimen tested was a beam clamped at both ends, but with the impacted end free to move longitudinally. The impact load had the shape of half a sine wave with a period *T*. (Weller et al., 1989) found out that for lower values of $2T/T_b$, (the ratio between the period of the applied loading and the period of the first free lateral vibration) the *knee* of the response curve tends to move away from the origin of the axes and flatten down. This indicates higher dynamic buckling loads. The analyses were done by using two different initial geometric imperfections. From figure (2.8) it is seen that a low $2T/T_b$-ratio indicates higher dynamic buckling loads, i.e. short loading durations gives high dynamic buckling loads.

The analysis was also done on a plate and gives the same results as for the beam. But as previously mentioned the dynamic buckling load is smaller than the classical characteristic bifurcation load for a corresponding perfect structure, when the load duration is close to the first natural period of lateral vibrations, see figure (2.9).

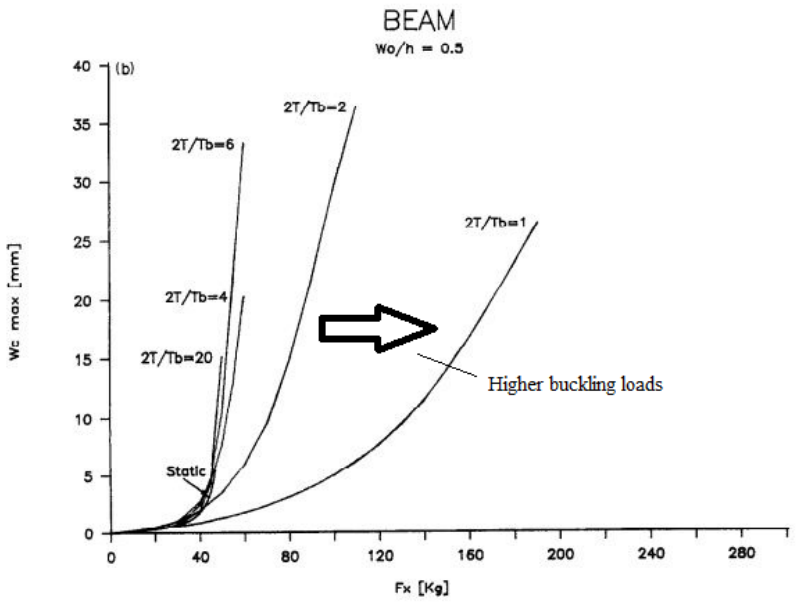

Figure 2.8: Effect of load duration on beams

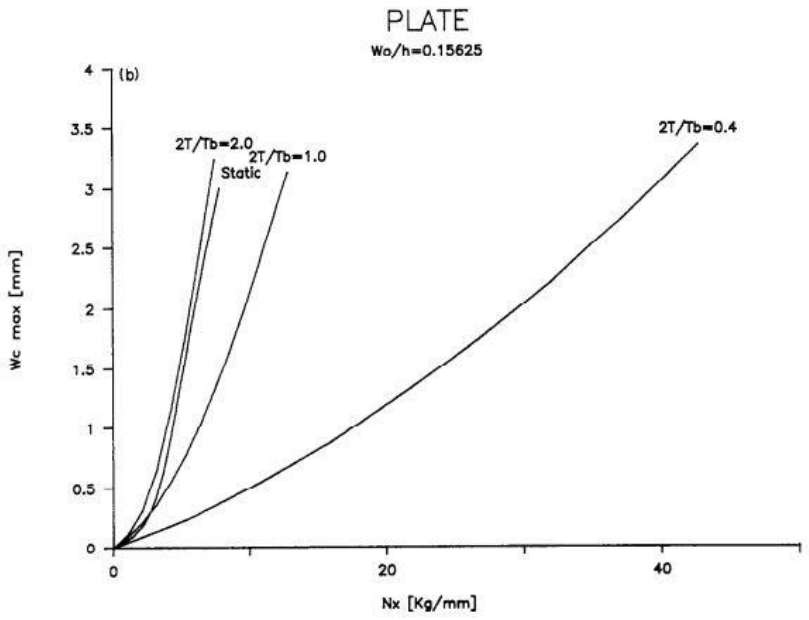

Figure 2.9: Effect of load duration on plates

The results obtained by (Weller et al., 1989) were confirmed by (Cui et al., 2002), see figure (2.10). The parameter α_{cr} is the buckling load amplification coefficient and t_0 is the load duration. It is seen that the buckling load amplification increases significantly as the duration of the loading decreases. λ is the reduced slenderness. The effect of reduced slenderness is investigated in section 2.4.3.

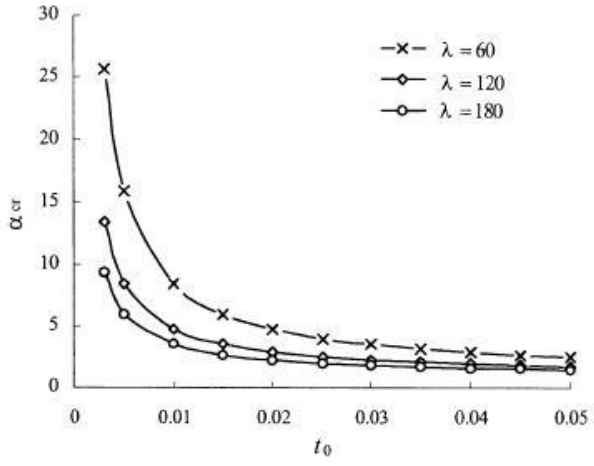

Figure 2.10: Buckling load amplification coefficient vs load duration

(Ekstrom, 1973) found out that a plate loaded rapidly will buckle at a higher critical stress than a plate loaded very slowly (statically). In the post-buckling phase the rapidly loaded plate

oscillates about the static load-deflection relation. This leads to higher stresses compared to the static case, see figure (2.11).

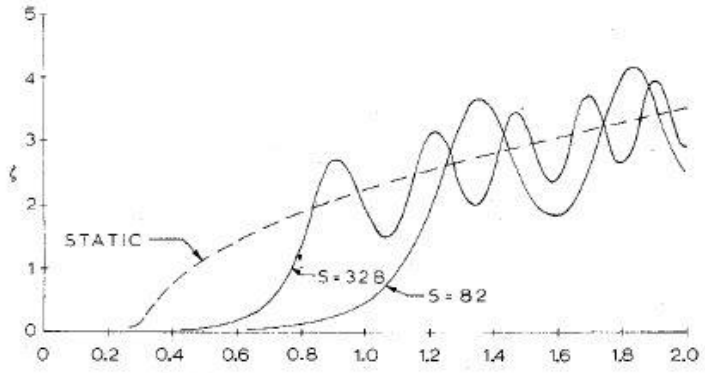

Figure 2.11: Response curves for different loading rates; S = 328, S = 82

2.4.2 Effect of initial imperfections

The effect of initial imperfections is also a factor worth investigating. (Weller et al., 1989) studied the initial imperfections effect on the dynamic buckling load on beams and plates. The analyses were performed by subjecting the components to an axial impact. The duration of the loading was kept constant. It was found that when increasing the ratio w_0/h , which is the initial imperfection divided over the elements length, the dynamic buckling load decreased, see figure (2.12). The buckling load is seen from the figure as the respective intersection of the branch of the curves in the *buckled state* with the applied load, F_x.

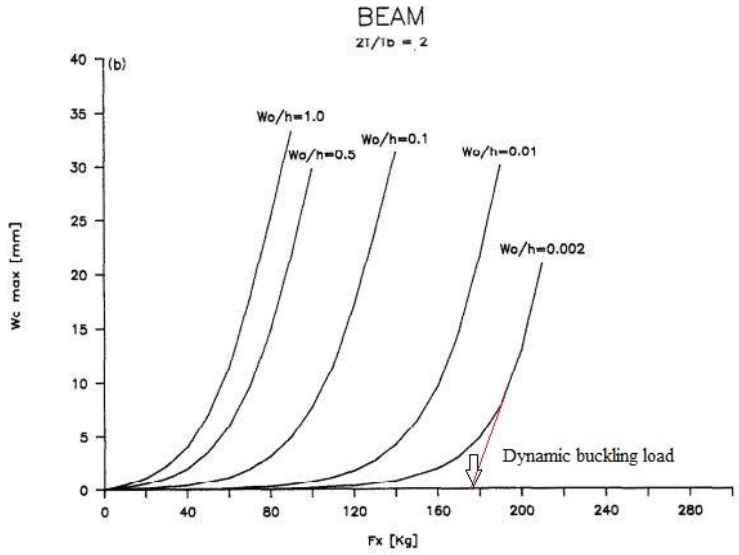

Figure 2.12: Effect of initial imperfections

(Ari-Gur, 1981) presented theoretical and experimental results for a rectangular plate impacted by a mass *m* moving in an in-plane direction, and concluded that the dynamic buckling load of the plate is strongly dependent on its initial geometric imperfection and the pulse duration. From the experiments performed by (Ari-Gur, 1981) it was obvious that the larger the initial imperfection, the smaller the maximum axial strain. This behavior is completely different from static buckling where the upper bound of the axial load is independent of the magnitude of the initial imperfection. This theory is confirmed by (Ekstrom, 1973) who found out that initial imperfections cause a decrease in the critical stress. Initial imperfections will also decrease the amplitude of the post-buckling oscillations.

2.4.3 Effect of reduced slenderness

(Cui et al., 2002) derived a dynamic buckling criterion, where an expression for the dynamic buckling critical load of a column where found.

$$\alpha_{cr} = 1 + \frac{34\sqrt{2}\pi^8 t_0^{-1}}{\lambda^2 \Omega} \tag{2.37}$$

From equation (2.37) it is seen that the buckling load is affected by different parameters. One of these parameters is λ, the slenderness of the column. Note that this is not the same as λ used by (Budiansky and Hutchinson, 1964) in the buckling criterion early in chapter 2. (Cui et al., 2002) plotted equation (2.37) and found out how the slenderness and the duration of the load affected the buckling load. The columns which were tested had initial imperfections ranging from 0,10 to 0,42mm.

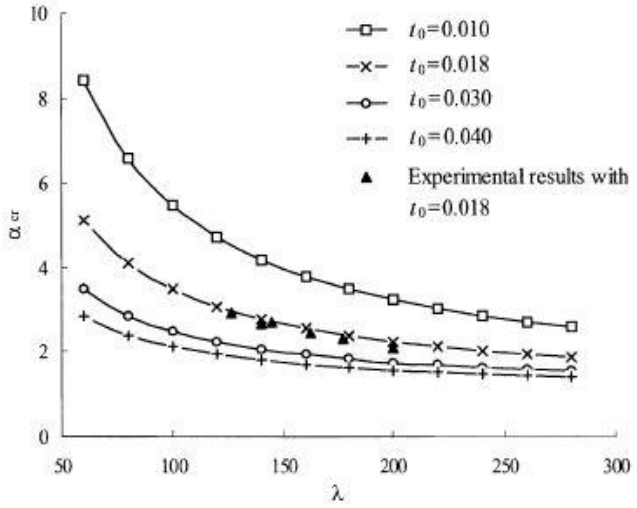

Figure 2.13: Effect of reduced slenderness

By investigating figure (2.13) it is seen that the buckling load is expected to decrease when increasing the columns slenderness. The reason for this is that a column with a small slenderness ratio will have a higher flexural stiffness compared to a column with high slenderness ratio. The importance of taking the reduced slenderness into account was confirmed by (Ari-Gur et al., 1982) who presented experimental results that showed that the magnitude of the dynamic buckling load of a column under axial impulse of a certain duration is determined by its slenderness ratio, see figure (2.14).

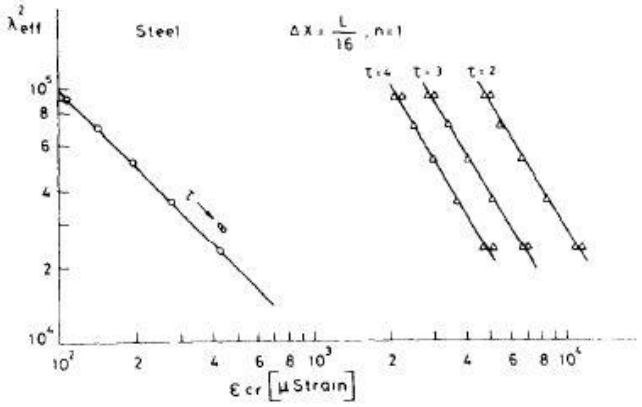

Figure 2.14: Critical strain vs. slenderness for steel columns

2.4.4 Effect of material choice

Steel is very much used in the marine industry, but in some cases there are other materials which are considered more suitable when designing a structure. Therefore it is important to investigate the effect of material choice with respect to dynamic buckling to make sure that the structure is safe. (Ari-Gur et al., 1982) performed several dynamic buckling tests with different materials. By plotting the dynamic load amplification factor (see section 2.4.5) versus the slenderness (figure 2.15), it was seen that the results for steel and aluminum alloy columns are within the same experimental scatter. It may then be concluded that material properties do not significantly affect the dynamic buckling behavior.

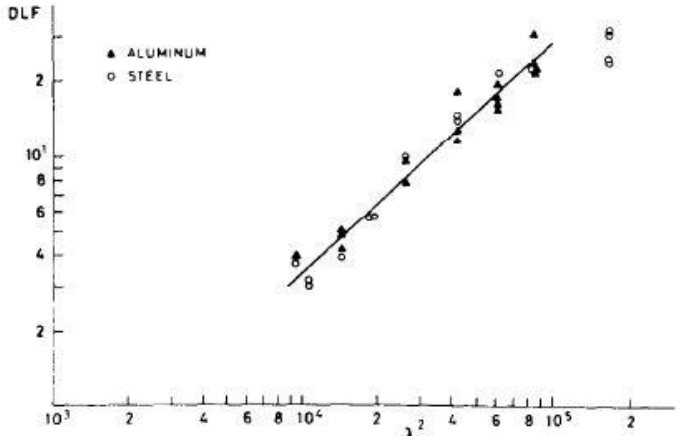

Figure 2.15: DLF versus slenderness for columns with different material properties

The statement that material properties do not affect dynamic buckling behavior was reinforced by the results of glass-epoxy specimens. This material consists of different materials throughout the column, and is defined as a composite material. These composite columns have different material properties in the axial direction and the properties differ also from those of the metal specimens. The experiments showed that the dynamic loading factor was not significantly affected when changing the material. Figure (2.16) shows the results for steel, aluminum and the composite material. The conclusion that materials properties do not significantly influence the dynamic buckling phenomenon is similar to that well known for static buckling of columns(Ari-Gur et al., 1982).

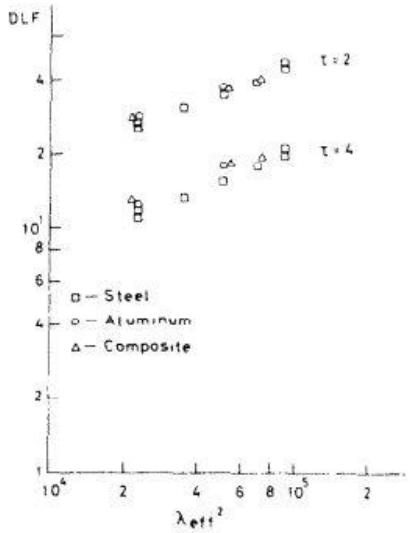

Figure 2.16: Effect of material choice on dynamic loading factor

2.4.5 Dynamic load factor (DLF)

The dynamic load factor is defined according to equation (2.38).

$$DLF = \frac{(P_{cr})_d}{(P_{cr})_s} \tag{2.38}$$

where $(P_{cr})_s$ is the static buckling load and $(P_{cr})_d$ is the dynamic buckling load. The concept of DLF is of practical interest for the designer, since it provides a direction indication of the load carrying capacity of the structural elements exposed to rapidly applied loads relative to almost statically applied loads (Weller et al., 1989). The analysis performed by (Weller et al., 1989) showed that both initial geometric imperfections and duration of the loading affect the DLF.

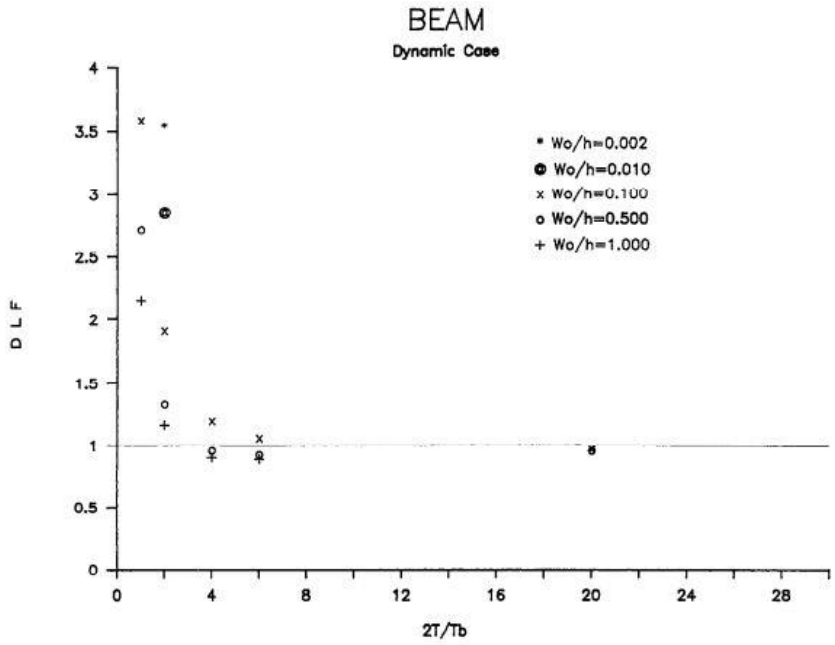

Figure 2.17: Effect of initial imperfections on DLF for various imperfections levels

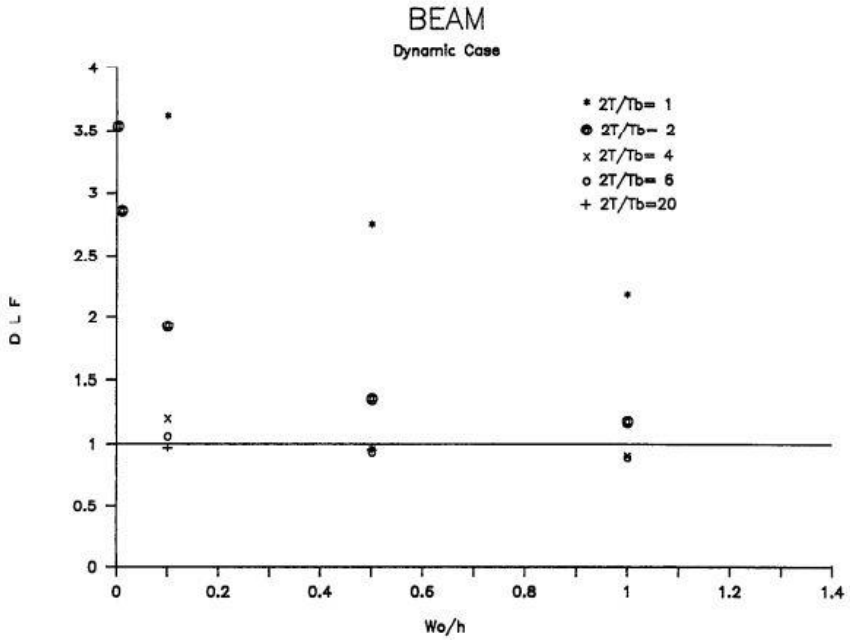

Figure 2.18: Effect of load duration on DLF for various load durations

From figure (2.17) and (2.18) it is seen that for $2T/T_b$ ratios above unity, the *DLF* is above 1. This indicates that the design of a structural element to sustain elastic static buckling is sufficient to withstand the impact loads. It is also observed that the *DLF* drops below unity for values $(2T/T_b) > 1$ and $(w_0/h) > 0.5$. This means that in some cases the dynamic buckling load does not exceed the static one. For a designer, this is an important phenomenon to be aware of.

Figure (2.17) and (2.18) coincides with the studies done by (Ari Gur and Weller, 1985) who found out that in the range of long-duration impacts, where the response is quasi-static and the dynamic buckling load approaches the static one, there is a possibility that for certain initial geometric imperfections of the plate the dynamic buckling load may drop below the static one. Further analysis of plates subjected to axial impacts showed that loading duration should be related to the natural period of free lateral vibration. In figure (2.19) the *DLF* is found by numerical methods performed by (Weller et al., 1989). It is seen that the *DLF* drops below unity as $(2T/T_b) > 2$, for certain values of initial imperfections. This is in correspondence with the *DLF* for beams shown earlier.

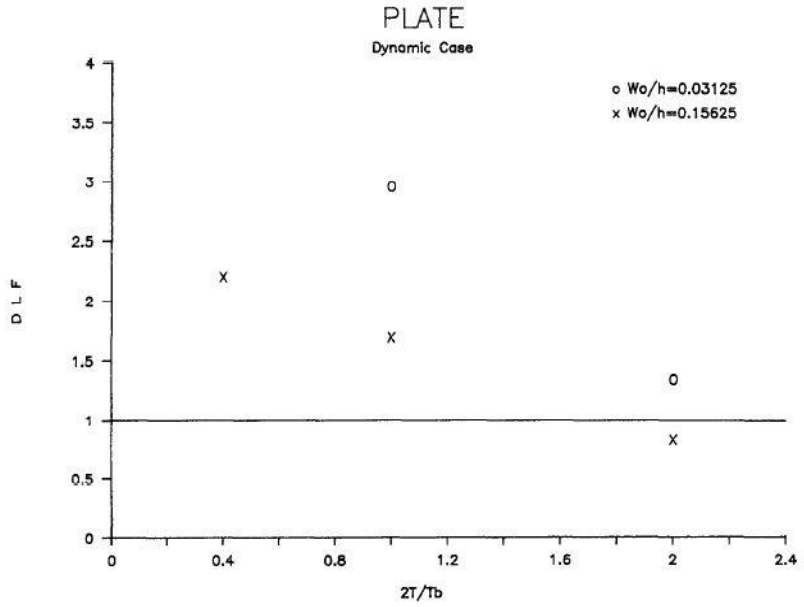

Figure 2.19: Dynamic load amplification factor for plates vs. duration of loading – numerical results

3 Dynamic analysis of a simple-beam column in *USFOS*

The computer program *USFOS* can be used to investigate dynamic buckling further. Following aspects are to be investigated in this section

- The transition from one buckling mode to a higher mode when the rate of loading is increased
- The sensitivity to the choice of initial imperfections, both with respect to total value as well as the relative composition of imperfection modes
- Effect of yielding on dynamic buckling loads

The validity of the analysis is examined by comparing results from *USFOS* with published analytical solutions. The analyses are done by considering a simple beam-column made of steel. The column is subjected to a nodemass with a constant initial velocity. The boundary conditions of the column are modelled with the impacting end of the column free to move longitudinally. The other end of the column is fixed from all translations, see figure (3.1).

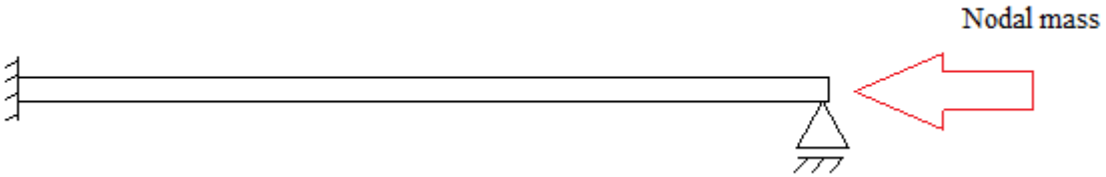

Figure 3.1: Column analysed in USFOS

3.1 Investigation of transition of buckling modes

As presented in the theory part, during pulse buckling it is observed that a band of preferred modes grows more rapidly than others. This is another feature that extinguishes pulse buckling from vibration buckling. The buckling modes in pulse buckling depends on the load and must be determined as a part of the solution(Lindberg, 2003).

To be able to investigate the transition from one buckling mode to a higher mode when the rate of loading is increased, the beam-column used in *USFOS* has to contain initial imperfections compatible with the three first buckling modes. Figure (3.2) shows how the three first buckling modes are summarized.

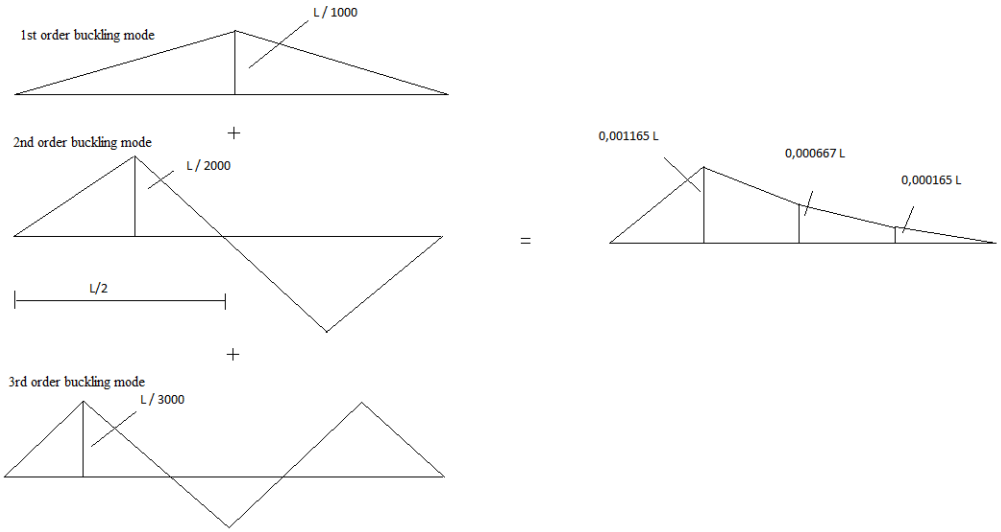

Figure 3.2: Summarizing all buckling modes

The analysis is performed by subjecting the beam-column to a loading consisting of a nodal mass with initial velocity. An analysis is run for different velocities and the buckling mode for each velocity is noted. The object is to find out when the transition between the different buckling modes occur. To increase the insight into dynamic buckling, the slenderness of the column is varied. The definition of slenderness is according to equation (3.1) (Amdahl, 2009).

$$\lambda = \sqrt{\frac{\sigma_Y}{\sigma_E}} \tag{3.1}$$

σ_Y is the yield stress, while σ_E is the *Euler* stress. The expression for the reduced slenderness can also be written according to equation (3.2).

$$\lambda^2 = \frac{\sigma_Y}{\sigma_E} = \sigma_Y \left(\frac{\pi^2 EI}{l_k^2 A} \right)^{-1} \tag{3.2}$$

The slenderness is varied by changing the length of the column. In the analysis lengths equal to 10m, 15m and 20m are used. The column is modeled by 4 elements of equal length. Table (3.1) shows the reduced slendernesses for the different columns.

Length [m]	**10**	**15**	**20**
Slenderness [-]	1,29	1,94	2,58

Table 3.1: Reduced slenderness

Table (3.2) shows the buckling modes of the column after subjecting the column with length equal to 10m to nodal masses with different initial velocity.

Velocity [m/s]	**Buckling mode**
0,2	1st
0,8	1st/2nd
1,0	2nd
6,0	2nd
8,0	2nd/3rd
10,0	3rd

Table 3.2: Velocity vs. transition between buckling modes, column with length = 10m

Figure (3.3) to figure (3.5) shows the different buckling modes for the column.

Figure 3.3: 1st order buckling mode

Figure 3.4: 2nd order buckling mode

Figure 3.5: 3rd order buckling mode

The values in table (3.2) are found by running an animation of the deformation of the beam-column in *USFOS*. By investigating this animation the buckling mode is found for each case. In some cases it is difficult to decide the velocity where the transition occurs. Therefore the results presented in table (3.2) should be taken with care. With this is mind the buckling loads for the transitions are according to table (3.3).

Buckling mode	**Velocity [m/s]**	**Buckling load [MN]**
1st → 2nd	0,9	2,8
2nd → 3rd	9,0	10

Table 3.3: Transition between buckling modes with associated velocities and buckling loads, column with length = 10m

Table (3.3) shows the velocities and the corresponding buckling loads where the transitions between the buckling modes occur. It is observed that it requires a significant increase in loading and velocity to elicit the 3rd order buckling mode. The problem can be investigated further by running the same analysis for columns with lengths equal to 15m and 20m, i.e. changing the slenderness.

Length	**Transition 1st → 2nd**		**Transition 2nd → 3rd**	
	Velocity [m/s]	Buckling load [MN]	Velocity [m/s]	Buckling load [MN]
15m	0,25	1,16	7,0	6,0
20m	0,18	0,75	5,0	3,8

Table 3.4: Transition between buckling loads for columns with lenghts equal to 15m and 20m

From table (3.4) it is seen that as the slenderness/length decreases the buckling load for the transition between the buckling modes decreases significantly. This coincides with the experiments done by (Ari-Gur et al., 1982), where the a column were subjected to an impulsive axial compression. The dynamic loading amplification factor was plotted against the slenderness, see fig. (3.6). Note that the magnitude of the *DLF* on the y-axis in fig (3.6) decreases as the y-coordinate increases.

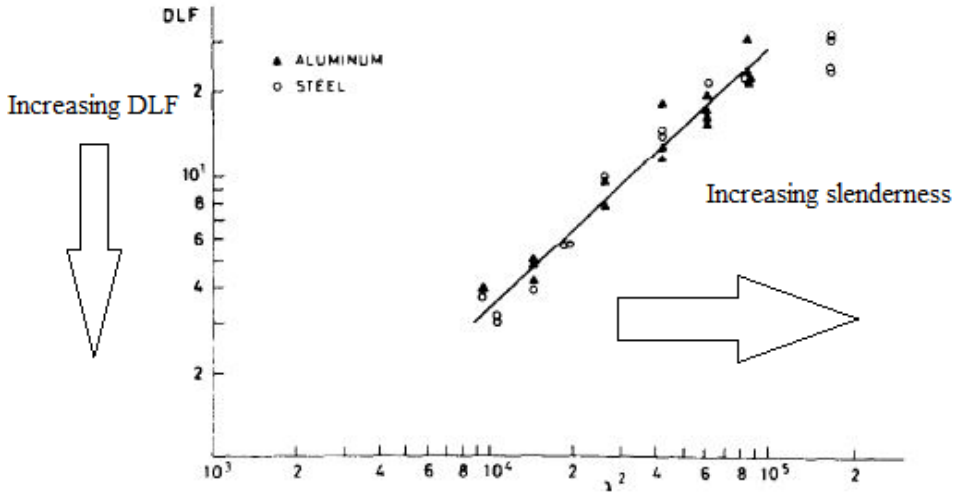

Figure 3.6: DLF versus slenderness for columns with different material properties.

It is seen that when the slenderness is increased the *DLF* is reduced. This is in correspondence with the results obtained in table (3.3) and (3.4).

3.2 Imperfection sensitivity analysis

A perfectly straight and symmetric column does not buckle under an axial impulsive compression. Real columns, however, are always imperfect and their dynamic buckling loads are dependent on the shape and the magnitude of their initial imperfection (Ari-Gur et al., 1982). Therefore, an imperfection sensitivity analysis is important when dealing with dynamic buckling. Factors worth investigating are the magnitude of the initial imperfections and the composition of imperfection modes.

3.2.1 Magnitude of imperfection

The analyses run in section 3.1 were done with imperfections with magnitude of order of 1\1000 times the columns length. In this section analysis with magnitudes of 1\100 and 1\10 of the length are conducted. The beam-column contains initial imperfections compatible with the three first buckling modes. The buckling loads are found by plotting the reaction force over the time history, one example is shown in figure (3.7). Results are tabulated in table (3.5) to (3.7).

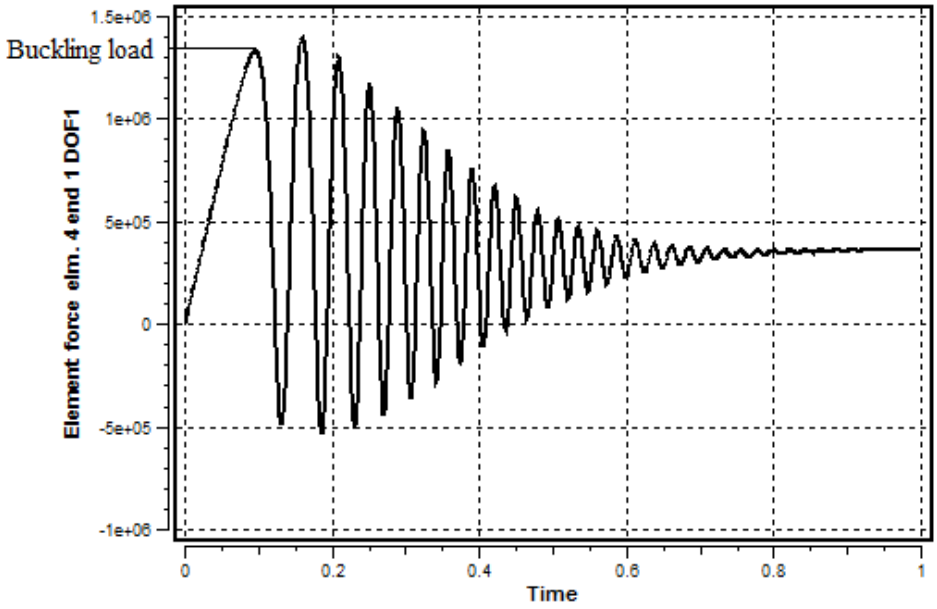

Figure 3.7: Buckling load for column from USFOS

Magnitude of imperfection [1/L]	Length of column [m]	Impacting velocity [m/s]	Buckling load [MN]
1/1000	10	0,2	1,900
1/100	10	0,2	1,250
1/10	10	0,2	0,450

Table 3.5: Imperfection analysis, column with length = 10m

Magnitude of imperfection [1/L]	Length of column [m]	Impacting velocity [m/s]	Buckling load [MN]
1/1000	15	0,2	1,100
1/100	15	0,2	0,370
1/10	15	0,2	0,028

Table 3.6: Imperfection analysis, column with length = 15m

Magnitude of imperfection [1/L]	Length of column [m]	Impacting velocity [m/s]	Buckling load [MN]
1/1000	20	0,2	0,850
1/100	20	0,2	0,225
1/10	20	0,2	0,030

Table 3.7: Imperfection analysis, column with length = 20m

From table (3.5) to (3.7) it is seen that the dynamic buckling load is significantly reduced when the magnitudes of the imperfections are increased. This agrees with the theory presented in section 2.4.2 where (Weller et al., 1989) found out that the dynamic buckling load decreases when the magnitude of the initial imperfections are increased, see fig. (3.8).

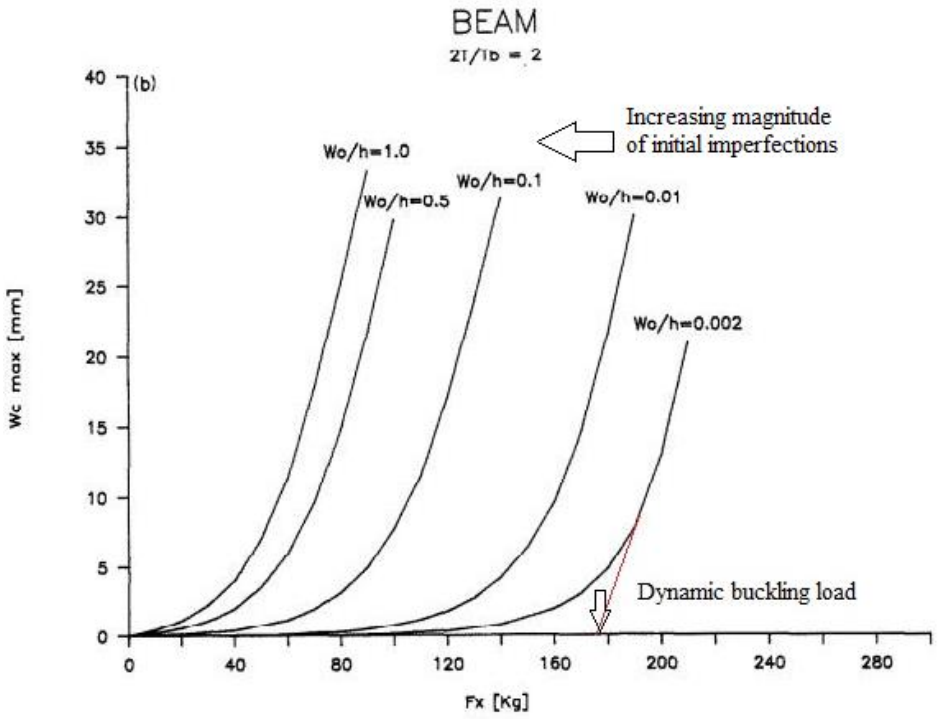

Figure 3.8: Effect on buckling load by changing magnitude of initial imperfections

3.2.2 Composition of buckling modes

Another aspect worth investigating is the composition of the buckling modes. In section 3.2.1 the analyses were done with implementing the three first buckling modes in the column. In this section it is investigated how the dynamic buckling load changes as buckling modes of higher order are added to the beam-column. Results are shown in table (3.8) to (3.10).

Buckling modes	Length [m]	Impacting velocity [m/s]	Buckling load [MN]
1st	10	0,2	1,32
1st + 2nd	10	0,2	1,25
1st + 2nd + 3rd	10	0,2	1,28

Table 3.8: Buckling loads with different composition of buckling modes, length = 10m

Buckling modes	Length [m]	Impacting velocity [m/s]	Buckling load [MN]
1st	15	0,2	1,18
1st + 2nd	15	0,2	1,07
1st + 2nd + 3rd	15	0,2	1,07

Table 3.9: Buckling loads with different composition of buckling modes, length = 15m

Buckling modes	Length [m]	Impacting velocity [m/s]	Buckling load [MN]
1st	20	0,2	1,15
1st + 2nd	20	0,2	0,82
1st + 2nd + 3rd	20	0,2	0,81

Table 3.10: Buckling loads with different composition of buckling modes, length = 20m

From table (3.8) to (3.10) it is seen that the buckling loads are reduced when buckling modes of higher order is added. It is also noted that the difference in dynamic buckling load when adding the 3rd buckling mode is small, compared to only implementing the 1st and 2nd order buckling mode.

3.3 Effect of yielding on dynamic buckling loads

The focus in the analyses done in section 3 has been to investigate how different factors influence the dynamic buckling load. To keep the beam-column out of its plastic zone, the analyses have been done by using an unrealistic high yield strength. To be able to run the

analyses with a realistic yield strength in *USFOS*, the time increment has to be decreased to 1\10000 of a second. The velocity of the initial nodemass is set to 0,2 m/s.

In this section the yield strength is set to a realistic value for steel. The purpose of the analysis is to investigate the effect this has on the dynamic buckling load for the beam-column. The yield strength used is equal to 240MPa, and buckling modes up to the 3rd order is implemented in the beam-column.

Length [m]	Buckling load [MN]
10	9,0E-07
15	9,0E-07
20	9,0E-07

Table 3.11: Buckling loads when using realistic yield strength

From table (3.11) it is seen that the buckling loads are equal for all the columns.

Figure (3.9) shows the buckling mode for the column with length equal to 10m. This buckling mode is also valid for the case with a column length equal to 15m and 20m. It should be noted that the magnitude of the displacements is reduced by a factor of 10 when the realistic value for the yield strength is used.

Figure 3.9: Buckling mode for column with length = 10m and σ_y = 240MPa

3.4 Comparison with hand calculations

To get an indication of the goodness of the results, it is possible to compare the results obtained in part 3 with calculations based on the buckling criterion developed by (Cui et al., 2002). By calculating the dynamic amplification factor and multiplying this with the static buckling load, the dynamic buckling load can be found.

First a static analysis in *USFOS* is performed. The beam-column is modelled with an initial geometrical imperfection equal to 1/1000 times the columns length. The results are tabulated in table (3.12).

Length [m]	10	15	20

Slenderness [-]	1,29	1,94	2,58
Buckling load [MN]	0,356	0,18	0,12

Table 3.12: Static buckling loads

The buckling criterion performed by (Cui et al., 2002) is based on the following equations.

$$\alpha_{cr} = 1 + \frac{34\sqrt{2}\pi^8 t_0^{-1}}{\lambda^2 \Omega} \tag{3.3}$$

where

$$\Omega^2 = \frac{n^4 \pi^4 C^2}{L^2 \lambda} \tag{3.4}$$

C is the stress wave velocity of the column, here defined according to equation (3.5).

$$C = \sqrt{\frac{E}{\rho}} \tag{3.5}$$

For the column with length equal to 10m, the buckling criterion gives the following results, see table (3.15).

Buckling mode	**1st order buckling mode**	**2nd order buckling mode**	**3rd order buckling mode**
Dynamic amplification factor	62	16	8
Dynamic buckling load [MN]	22,1	2,88	0,96
Dynamic buckling load found from USFOS [MN]	1,32	1,58	1,60

Table 3.13: Comparison between results from USFOS and from buckling criterion

The dynamic buckling loads determined from the buckling criterion developed by (Cui et al., 2002) does not fit very well with the results obtained in *USFOS*. A reason for this could be that (Cui et al., 2002) tested equation (3.3) for large slenderness values ($\lambda > 50$). The column with length equal to 20m has the largest slenderness value of the column tested ($\lambda = 2{,}58$), but is still well outside this range. It may therefore be possible that this approach is not valid for components will low values of reduced slenderness. It should also be noted that the load durations used by (Cui et al., 2002) are very small compared to the duration used in the

analysis performed in chapter 3. From figure (3.10) it is seen that the amplification factor decreases as the load duration increases, and it can be seen that the factor becomes constant for high load durations.

(Cui et al., 2002) developed the buckling criterion for columns with imperfections in the range of 0,1mm to 0,42mm, i.e. they can be considered as straight columns. The columns analyzed in *USFOS* have imperfections in the range of 1/1000 times the length, which for the column with length equal to 10m results in an imperfection of 10mm. This can also be a reason why the analytical results do not coincide with results obtained in *USFOS*.

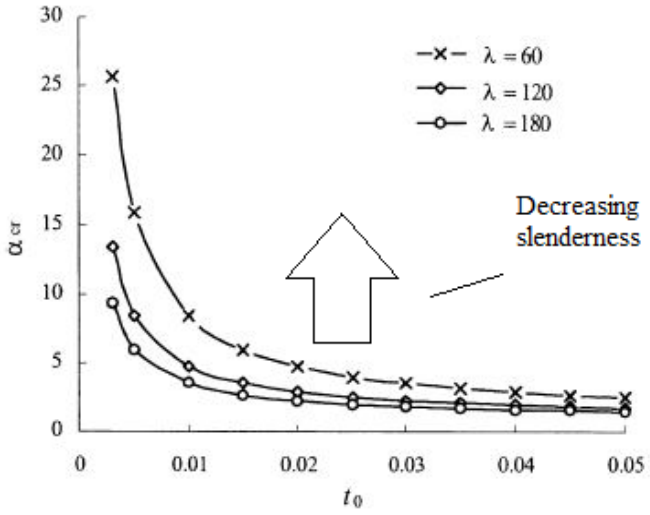

Figure 3.10: Buckling load amplification coefficient vs. load duration

This procedure was also shown in the project work (Landa, 2013), but could still be used as an indication on dynamic buckling loads for components with high slenderness and small values of initial imperfections.

3.5 Discussion

For the analyses done with the beam column the results indicate that the impacting velocity which defines the transition between one buckling mode to a higher mode varies, when the reduced slenderness of the column is changed. It was observed that the transition from the 1st to 2nd buckling mode occurred at low impacting velocities. To elicit the 3rd buckling mode the velocity of the impacting mass has to be significantly increased. The results are in good correspondence with the work conducted by (Ari-Gur et al., 1982). This work indicated that by decreasing the slenderness/length of the column, the dynamic loading factor will increase.

The results also indicate that the magnitude of imperfections is an important factor to take into account when dealing with dynamic buckling. It was experienced that the buckling loads decreased when the magnitude of imperfections were increased. By comparing the results from different values of reduced slenderness it is observed that the reduction in dynamic buckling loads increases as the reduced slenderness decreases. This is shown in table (3.14).

Magnitude of imperfection [1/L]	**Percentage reduction in dynamic buckling loads [%]**		
	Reduced slenderness [-]		
	1,29	1,94	2,58
1/1000 to 1/100	34	67	74
1/100 to 1/10	64	92	87

Table 3.14: Percentage reduction in dynamic buckling loads when changing magnitude of imperfection

From table (3.14) it is observed that the percentage reduction on the dynamic buckling loads increases when the reduced slenderness in increased, i.e. length of column increased. Except for the change of magnitude of imperfection from L/100 to L/10 for the column with length equal to 20m, the results indicate that an increase in magnitude of imperfections combined with an increase in slenderness will lead to a significant decrease in dynamic buckling loads.

It was also experienced that the dynamic buckling loads were affected by the composition of the buckling modes. Table (3.15) shows the percentage reduction in dynamic buckling loads for the different combinations of buckling modes.

Buckling modes	**Percentage reduction in dynamic buckling loads [%]**		
	Reduced slenderness [-]		
	1,29	1,94	2,58
1^{st} vs. 1^{st} + 2^{nd}	5	9	29
1^{st} + 2^{nd} vs. 1^{st} + 2^{nd} + 3^{rd}	-2	0	1

Table 3.15: Percentage reduction in dynamic buckling loads when changing the combination of buckling modes

Table (3.15) shows that the introduction of the 2^{nd} order buckling mode leads to a decrease in the dynamic buckling load. The magnitude of the decrease increases as the slenderness increases. The change in the dynamic buckling load when the 3^{rd} order buckling mode is

introduced is small. A reason for this can be that the magnitude of the 3rd order buckling mode was small compare to the 1st and 2nd order buckling modes. Considering the results from table (3.4), where the large transition velocity from the 2nd order buckling mode to the 3rd order buckling mode was observed, the results are expected. To be able to elicit the 3rd order buckling mode the velocity of the impacting mass has to be significantly increased.

From the analyses where the effect of yielding was investigated it was experienced that the buckling loads were significantly reduced when a realistic value for the yield strength was used. The dynamic buckling loads were constant for all slendernesses. This can be questioned when looking at the previous results from this section. The reduced slenderness has a major influence on the dynamic buckling loads. This is confirmed by (Ari-Gur, 1981) who concluded from experimental results that the magnitude of the dynamic buckling load of a column under axial impulse of a certain duration is determined by its slenderness ratio.

4 Dynamic analysis of a simply supported plate in *ABAQUS*

ABAQUS can be used to analyze a simply supported plate with constrained boundaries and varying slenderness. The plate is modeled by using shell modeling. The plate is simply supported with constrained boundaries, i.e. all edges of the plate are set to remain straight during the analysis.

By performing an eigenvalue analysis the eigenmodes of the plate is obtained. The eigenmodes are implemented as initial imperfections in the plate. Following problems are to be investigated in the analysis.

- Mesh size convergence study
- The transition from one buckling mode to a higher mode when the rate of loading is increased
- Sensitivity to choice of initial imperfections, both with respect to total value as well as the relative composition
- Effect of yielding on the dynamic buckling loads

The results obtained in *ABAQUS* are also compared to results from an analytical solution. This analytical solution is found by using the theory developed by (Ekstrom, 1973), see section 4.6.

The plate used in *ABAQUS* is a rectangular plate, see fig (4.1). As for the column analyzed in chapter 3, an unrealistic high yield strength is used, to keep the plate in the elastic zone throughout the analyses. Analyses with using a realistic value for the yield strength are done in section 4.7.

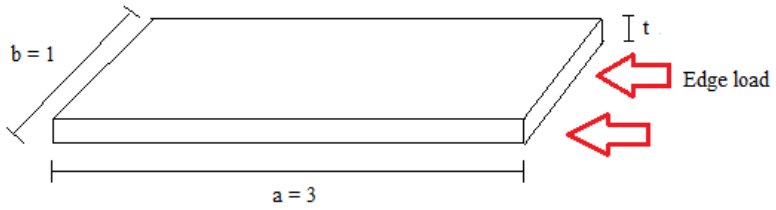

Figure 4.1: Plate

With the dimensions shown in figure (4.1), the aspect ratio of the plate is equal to 3. The thickness of the plate is varied, which means that the reduced slenderness also varies. In the analyses the thickness used are 10mm, 15mm and 20mm. As for the column analyzed in chapter 3, the plate is hit with a load that has an initial velocity. In *ABAQUS* this can be modeled by using an edge load. The impacting velocity is varied to investigate different phenomena connected to dynamic buckling. The duration of the analysis is set to 2 seconds.

4.1 Mesh size convergence study

To obtain acceptable results in *ABAQUS* it is important to generate a good mesh of elements. The plate considered is simple without stiffeners, so the mesh size is equal over the whole plate. Small elements lead to long computational times, and too large elements will lead to inaccurate results. With this is mind, a mesh size convergence study has been performed to obtain the optimal mesh size for the current problem.

It is also important to choose the correct element type. There are several options in *ABAQUS* and in this report the element type used is the *S4R-elements*. With these elements reduced integration is used. This will reduce computational time and may lead to improved accuracy of the computed finite element results (softens the behavior) (Mathisen, 2011).

The mesh size convergence study is done by varying the mesh size and observing the convergence of the results, i.e. buckling load and stresses. It is also important that the mesh size is able to describe the initial imperfections properly. The three first eigenmodes of the plate are to be implemented in the model as initial imperfections. Figure (4.2) and (4.3) shows both the deformed and undeformed shape of the plate when a coarse mesh is used.

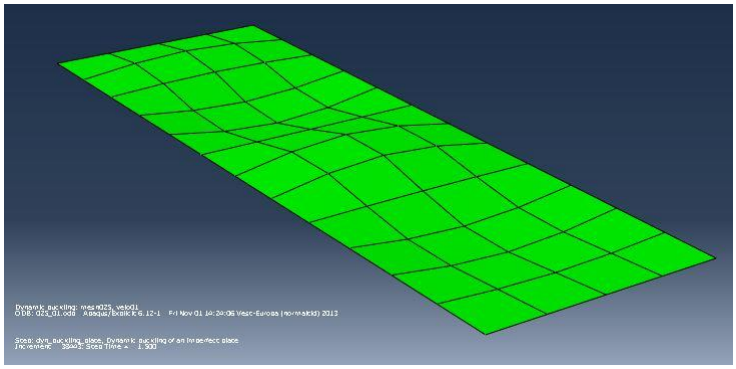

Figure 4.2: Mesh = 0,25m, undeformed shape

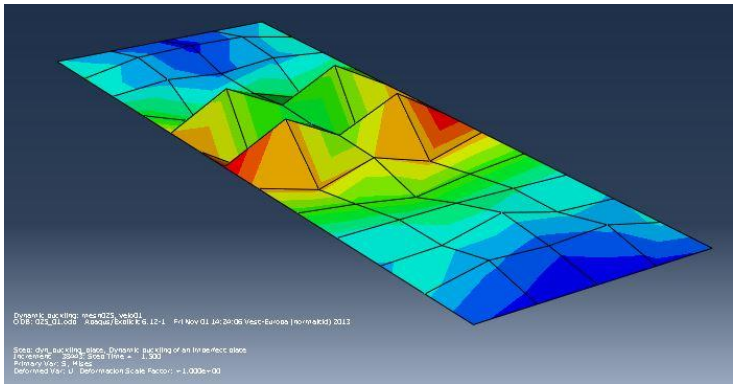

Figure 4.3: Mesh = 0,25m, deformed shape, distribution of von Mises stress

It is seen from figure (4.2) and (4.3) that a coarse mesh is not able to describe the deformations of the plate to an acceptable level of accuracy. A finer mesh is needed, and figure (4.4) and (4.5) shows the deformed and undeformed plate with an acceptable mesh size.

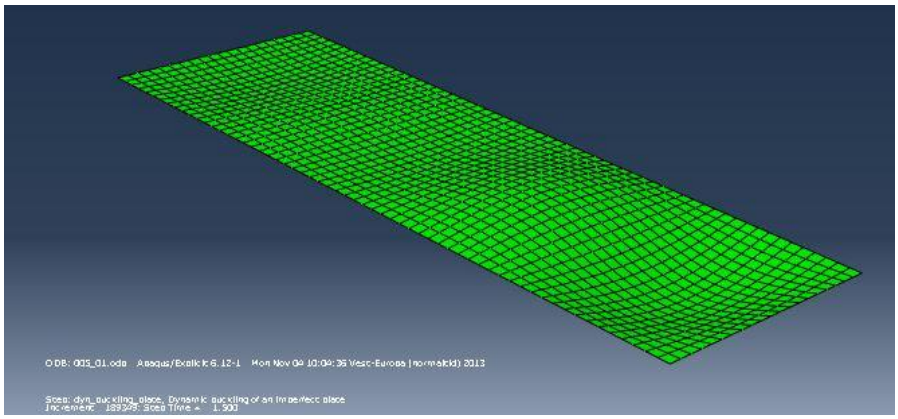

Figure 4.4: Mesh 50mm, undeformed

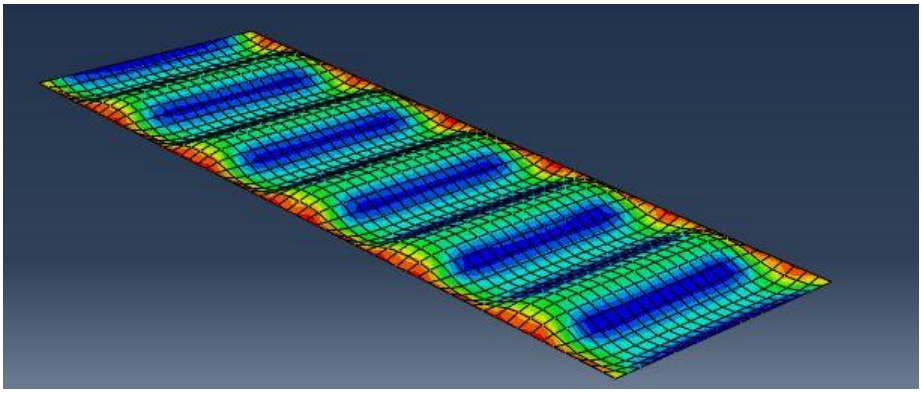

Figure 4.5: Mesh 50mm, deformed shaped, distribution of von Mises stresses

From figure (4.4) and (4.5) it is seen that a mesh size equal to 50mm is able to describe both the deformed and undeformed shape well enough. It is also necessary to run further analysis with this mesh when changing the initial velocity of the edge load. The reason for this is that it is expected that the deformation patterns complexity increases when the velocity is increased.

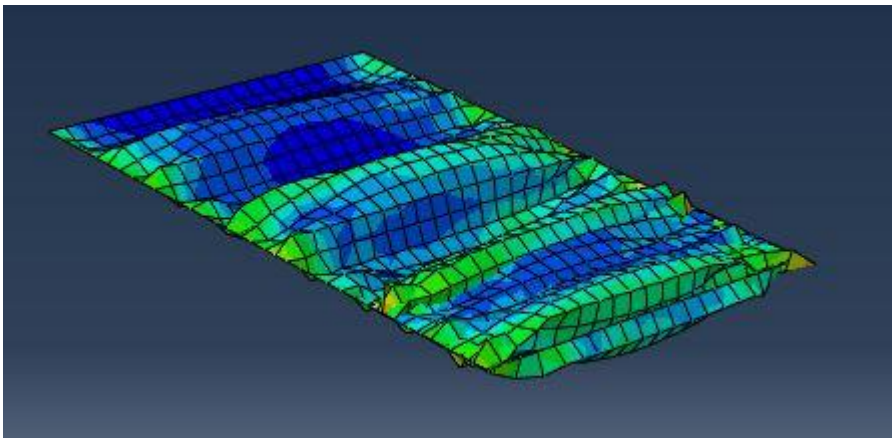

Figure 4.6: Mesh 50mm, velocity = 1m/s

From figure (4.6) it is seen that the deformation of the plate when the velocity of the edge load is equal to 1m/s is significant. The mesh size is however still acceptable. When the velocity is increased to 2m/s, the deformation of plate is of a major size, but the mesh size is still able to describe stresses and translations well.

As previously written the mesh shall also be capable to describe the eigenmodes of the plate with a sufficient level of accuracy. But since a mesh size equal to 50mm is able to describe the deformation pattern for the dynamic analysis well, it is assumed that the eigenmodes are described well enough with the same mesh size. When the mesh size is changed to 40mm, the

results are the same as for a mesh size equal to 50mm. A mesh size of 50mm is therefore used in this report.

4.2 Eigenvalue analysis

An eigenvalue analysis has to be performed to be able to introduce imperfections to the plate. A static buckling analysis can be run in *ABAQUS* to find the 8 first eigenmodes. The analyses are performed with a mesh size equal to the one found in the mesh size convergence study in section 4.1, i.e. 50 mm. Figure (4.7) to (4.10) shows the 5 first eigenmodes.

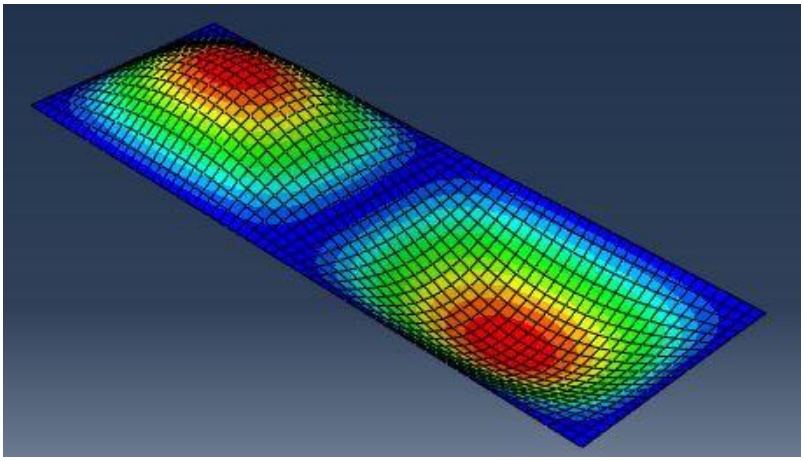

Figure 4.7: Eigenmode 1, 2 halfwaves

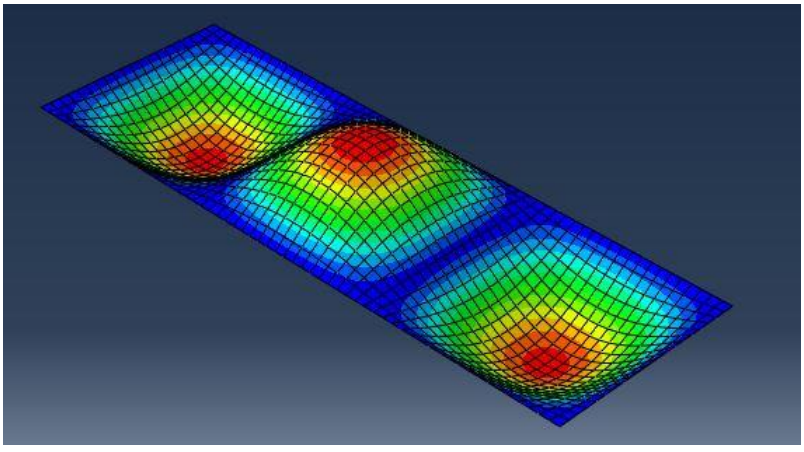

Figure 4.8: Eigenmode 2, 3 halfwaves

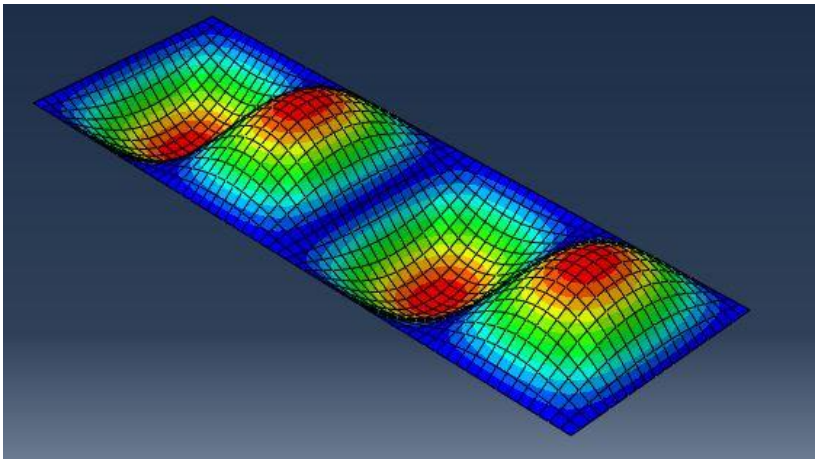

Figure 4.9: Eigenmode 3, 4 halfwaves

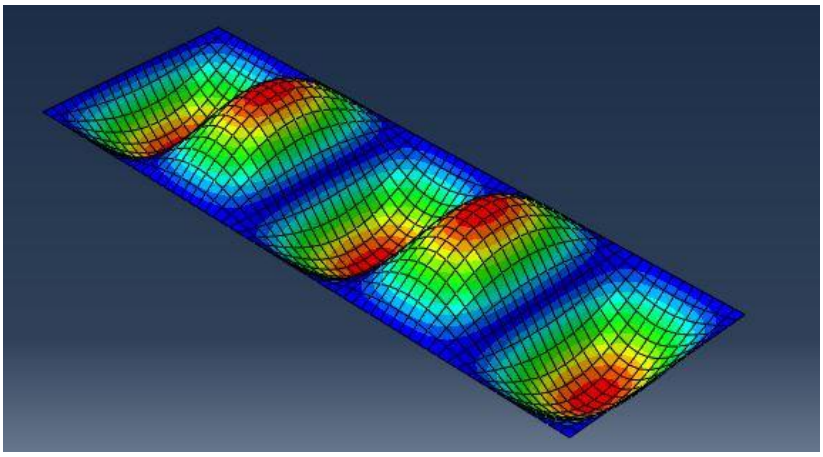

Figure 4.10: Eigenmode 4, 5 halfwaves

The eigenmodes showed above is combined and implemented as initial imperfections, and are as previously mentioned combined and implemented as initial imperfections. Figure (4.11) shows the imperfect plate, when the eigenmodes shown above is combined, i.e. the first 4 eigenmodes.

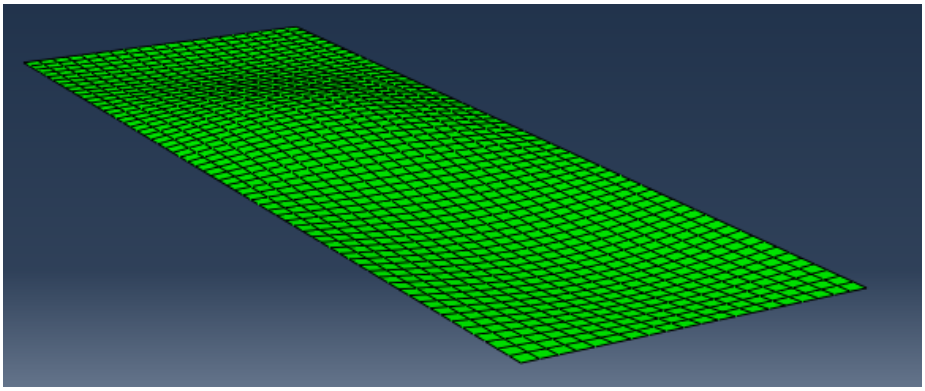

Figure 4.11: Eigenmode 1 to 4 combined

An overview of the remaining eigenmodes calculated from *ABAQUS* can be found in table (4.1).

Eigenmode	Number of half-waves
1	2
2	3
3	4
4	5
5	6
6	7
7	8
8	9

Table 4.1: Overview of eigenmodes

4.3 Dynamic analysis: Effect of reduced slenderness

As for the column considered in chapter 3, it is of interest to investigate the effect of changing the reduced slenderness of the plate, i.e. changing the thickness of the plate, see equation(4.1).

$$\beta = \frac{b}{t}\sqrt{\frac{\sigma_y}{E}} \tag{4.1}$$

Note that the notation for the reduced slenderness is changed from chapter 3, where λ was used. The thicknesses used are 10mm, 15mm and 20mm. This gives the following values for the reduced slenderness, see table (4.2).

Thickness [mm]	b [mm]	σ_y [MPa]	E [MPa]	Reduced slenderness [-]
10	1000	240E+16	2.1E+11	3,45
15	1000	240E+16	2.1E+11	2,30
20	1000	240E+16	2.1E+11	1,73

Table 4.2: Reduced slenderness

Different analyses can be performed in *ABAQUS* to investigate the effect of changing the slenderness of the plate. First, the analyses are performed with keeping the initial velocity of the edge load constant. Later, the velocity and duration of the load can be varied to investigate the problem thoroughly. Initial imperfections are implemented, and eigenmodes 1, 2, 3 and 4 are used, i.e. eigenmodes with 2, 3, 4 and 5 half-waves. The eigenmodes are scaled according to table (4.3).

Eigenmode	Scaling, i.e. max amplitude [mm]
1st	3
2nd	2
3rd	1
4th	0,5

Table 4.3: Scaling of initial imperfections (eigenmodes)

The buckling loads are found by plotting the reaction force over the time history for the edge parallel to the loaded edge, see figure (4.12).

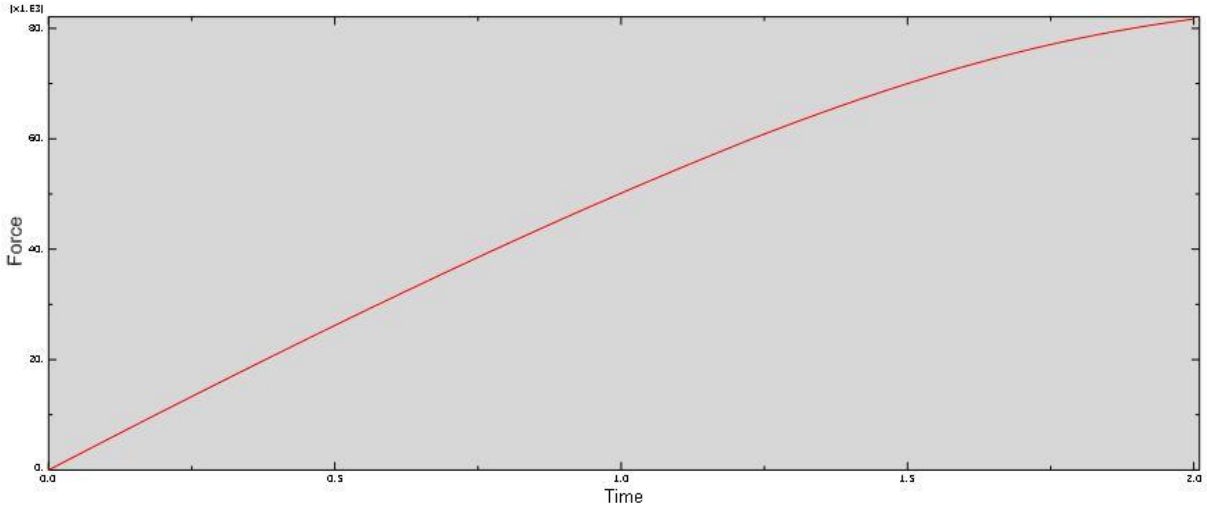

Figure 4.12: Reaction force for edge parallel to loaded edge

Thickness [mm]	Reduced slenderness	Buckling load [kN]
10	3,45	17,20
15	2,30	66,70
20	1,73	131,90

Table 4.4: Buckling load for different values of thickness (reduced slenderness)

The buckling loads in table (4.4) indicate that a decrease in reduced slenderness (increasing the thickness) leads to a significant increase in the buckling load. This is the same as for the column investigated in chapter 3 and coincides also with the theory presented in section 2.4.3. Here, (Cui et al., 2002) presented figure (4.13) which shows the relation between reduced slenderness and buckling load.

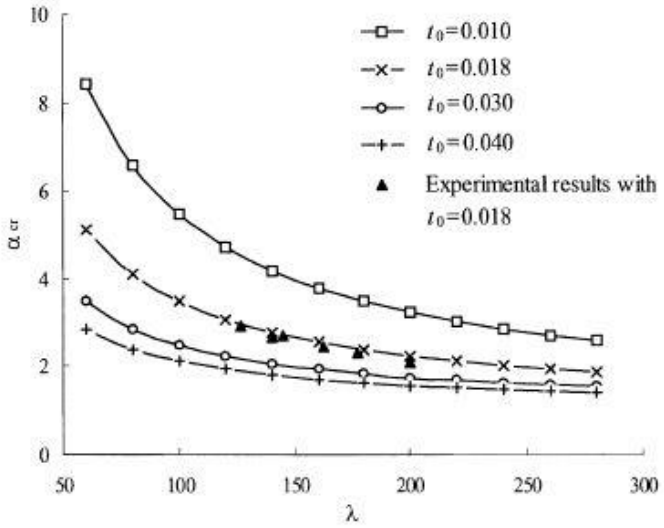

Figure 4.13: Reduced slenderness vs. critical load

It is interesting to investigate the buckling modes for the different values of reduced slenderness, see figure (4.14) to (4.16).

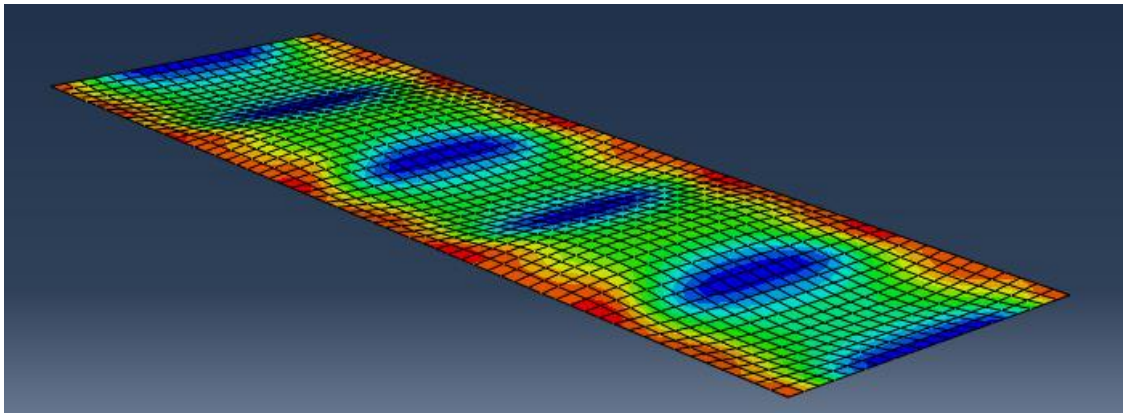

Figure 4.14: Buckling mode, thickness = 10mm

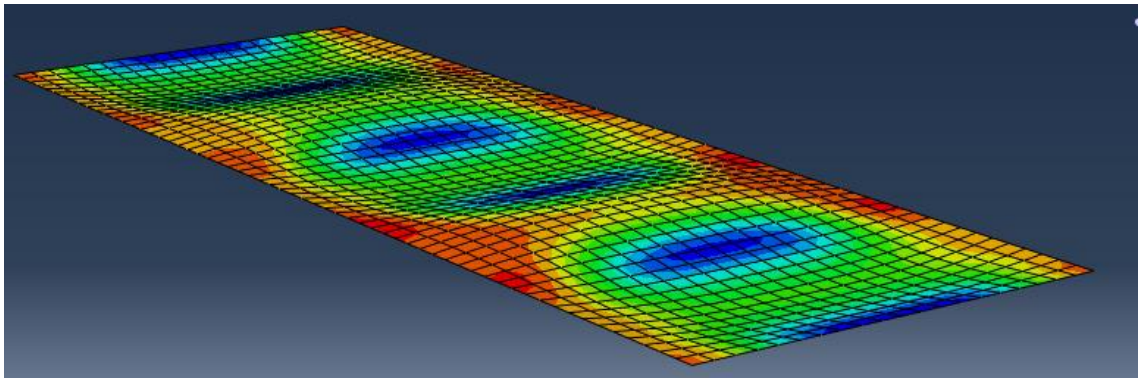

Figure 4.15: Buckling mode, thickness = 15mm

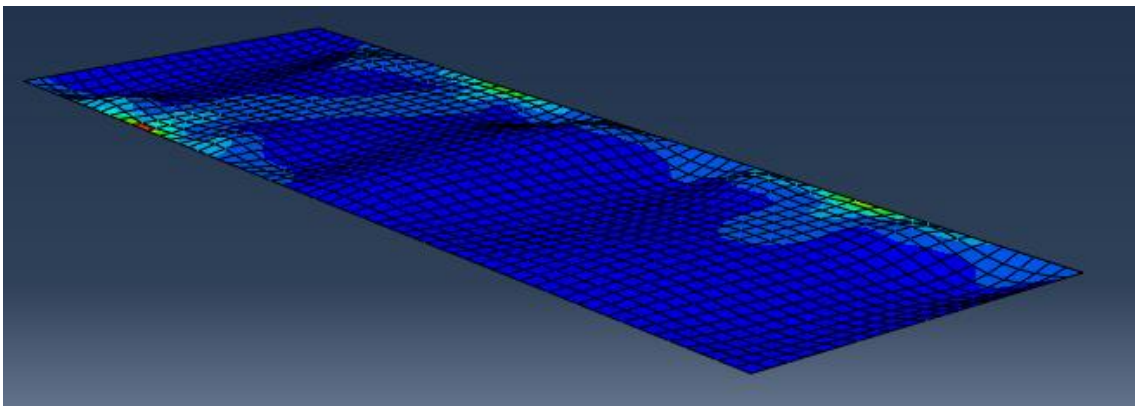

Figure 4.16: Buckling mode, 20mm

As earlier mentioned the velocity can be varied to investigate further aspects regarding variation of reduced slenderness. Results are shown in figure (4.17).

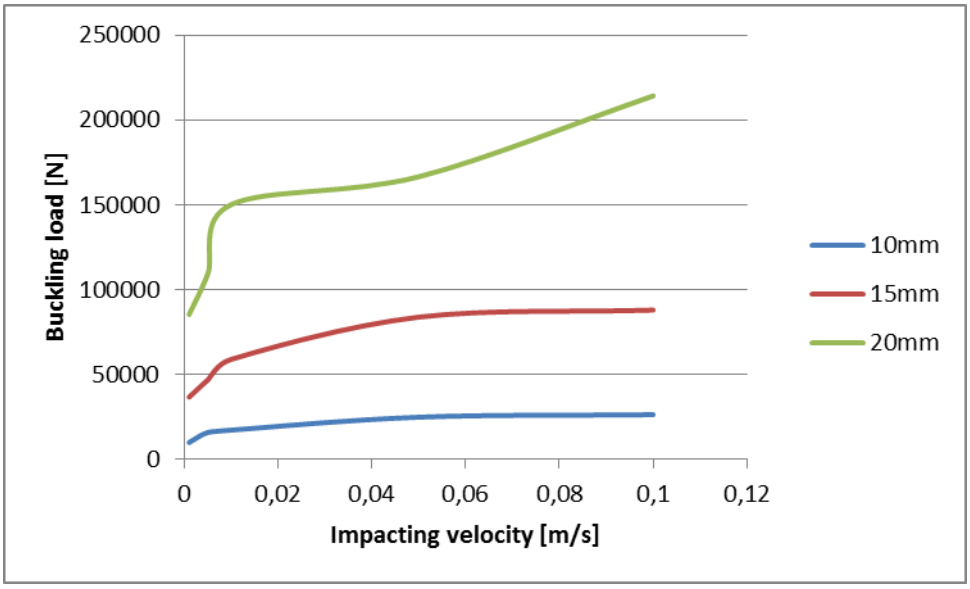

Figure 4.17: Buckling load vs. impacting velocity for different values of plate thickness (reduced slenderness)

4.4 Investigation of transition of buckling modes

It is of interest to investigate the dominant buckling modes when the plate is subjected to an edge load with an initial velocity. The analysis is done by combining the eigenmodes found in section 4.2, and us these as initial imperfections. The velocity of the edge load is varied, and the buckling mode is investigated. Table (4.6) shows the buckling mode of the plate when the impacting velocity is varied. To increase the insight of the problem, several combinations of the eigenmodes are analyzed. The scaling of the different eigenmodes is also varied. The scaling is showed in table (4.5).

Combination	Eigenmodes	Scaling, i.e. amplitudes of eigenmodes [mm]
1	1 + 2 + 3 + 4	1: 3 2: 2 3: 1 4: 0,5

2	1 + 2 + 3 + 4	1: 3 2: 3 3: 3 4: 3
3	2	1: 3

Table 4.5: Overview of combinations of eigenmodes and respective scaling

.

	Velocities[m/s]								
Combination	**0,001**	**0,002**	**0,004**	**0,005**	**0,0075**	**0,01**	**0,05**	**0,1**	**1,0**
1	3	4	5	5	5	5	9	11	Deformed
2	3	5	5	5	5	5	9	9	Deformed
3	3	3	5	5	5	5	8	11	Deformed

Table 4.6: Number of halfwaves in buckling mode for different combinations of eigemodes vs. velocity of edge load, plate with thickness = 10mm

It is seen from table (4.6) that for high impacting velocities, the plate buckles in buckling modes of high order that are not included in the analysis. At a velocity equal to 1 m/s the plate is fully deformed and the displacement in the longitudinal direction is significant. Another aspect worth investigating is the buckling load for the different combinations of eigenmodes. Figure (4.18) shows the buckling loads for the combinations.

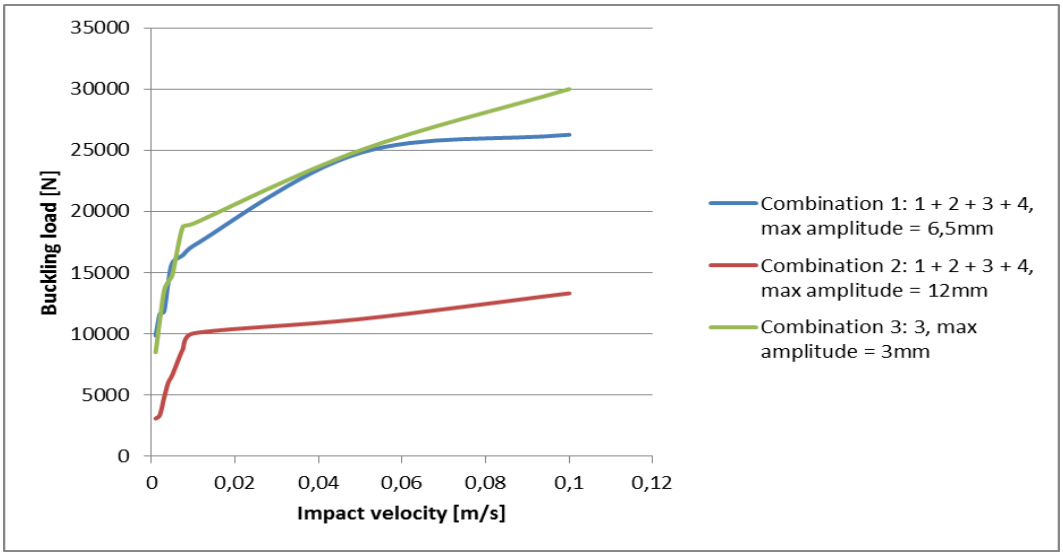

Figure 4.18: Buckling load vs. impact velocity

Figure (4.18) shows that the buckling loads for combination 1 and combination 3 are in the vicinity of each other, while the buckling loads for combination where all the eigenmodes were scaled equally are at a lower level. These results indicate that the scaling and combinations of the imperfections have a major influence on the buckling load.

4.5 Imperfection study

In the previous analyses the plate has been modeled with initial imperfections. The shape of the first buckling mode for the plate can be found from figure (4.19) when the aspect ratio is known. The length of the plate has been set to 3m, while the width is equal to 1m. This means that the aspect ratio is equal to 3. From figure (4.19) it is found that m = 3. This indicates that the buckling mode for the plate consists of three sine halfwaves. From theory presented in (Amdahl, 2009) it is shown that when the plate buckles in this form, the lowest buckling load is found.

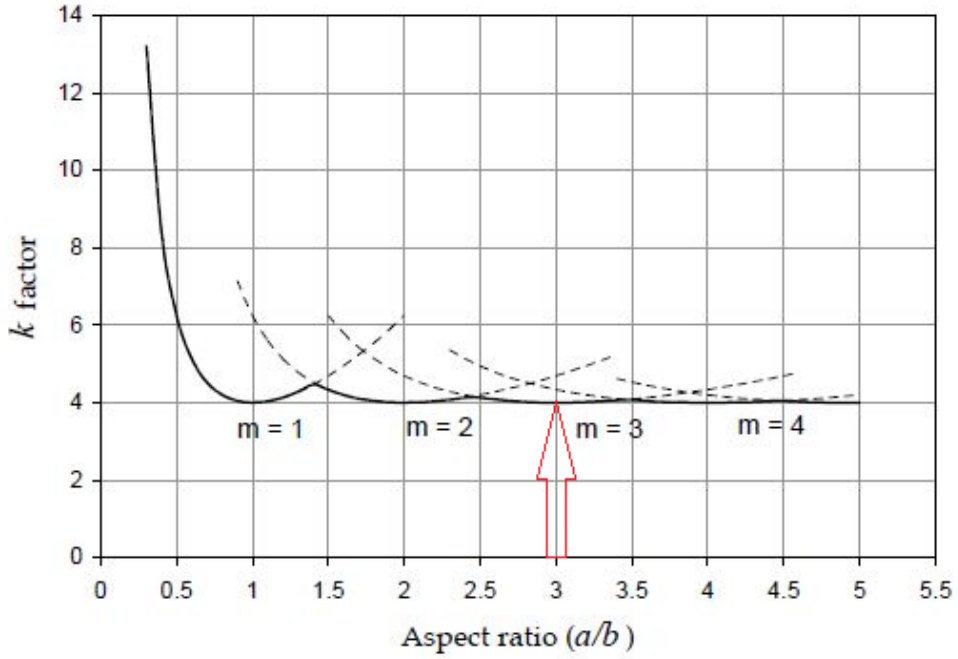

Figure 4.19: Buckling coefficient versus plate aspect ratio

Another aspect worth investigating is the behavior of the plate when buckling modes of higher order are implemented in the analysis. This was investigated in section 4.3, and it was found that the combination and scaling of the imperfections had a major influence on the buckling load. To investigate the problem further, multiple analyses are conducted in *ABAQUS.*

4.5.1 Combinations of eigenmodes

Figure (4.18) indicates that the choice of combinations of eigenmodes implemented as initial imperfections affects the buckling load of the plate. In this section different combinations of eigenmodes are analyzed. The scaling of the eigenmodes is similar for all combinations, while the velocity of the impacting edge load is constant equal to 0,005 m/s. The analysis is performed on a plate with thickness equal to 10mm.

Eigenmodes in combination	**Number of half-waves in buckling mode**	**Buckling load [kN]**
1	4	21
1 + 2	5	18
1 + 2 + 3	5	16

1 + 2 + 3 + 4	5	15
1 + 2 +…+ 5	5	15
1 + 2 +…+ 6	5	15
1 + 2 +…+ 7	5	15
1 + 2 +…+ 8	5	15

Table 4.7: Buckling loads for different combinations of eigenmodes

From table (4.7) it is seen that when buckling modes with higher order are introduced, the buckling load decreases. The buckling load is however approximately constant after the 4th order buckling mode is introduced (5 halfwaves). The reason for this can be that the scaling of buckling modes after the 4th order is very small. The scaling of the buckling modes are done according to table (4.8).

Buckling mode	**Scaling, i.e. max amplitude [mm]**
1st	3
2nd	2
3rd	1
4th	0,5
5th	0,25
6th	0,125
7th	0,0625
8th	0,03125

Table 4.8: Scaling of eigenmodes

4.5.2 Scaling of eigenmodes

Results presented in section 4.4 and 4.5.1 predicts that the scaling of the different eigenmodes affects the buckling load. Therefore, several analyses with different scaling of eigenmodes are performed in *ABAQUS*. During the analyses combination 1 of eigenmodes is used, i.e. eigenmodes with 2, 3, 4 and 5 half-waves summarized. The analysis is performed with a plate

with thickness equal to 10mm. Table (4.9) shows the different combinations of scaling used in the analyses.

Combination of scaling	Amplitude [mm]				Maximum amplitude [mm]
	Eigenmode 1 2 half-waves	Eigenmode 2 3 half-waves	Eigenmode 3 4-halfwaves	Eigenmode 4 5 half-waves	
1	3	2	1	0,5	6,5
2	3	3	3	3	12
3	1	1	1	1	4
4	0,5	3	0,5	0,5	4,5
5	0,5	1	2	3	6,5

Table 4.9: Overview of different scaling of eigenmodes

Combination of scaling	Buckling load [kN]
1	12,35
2	6,66
3	12,34
4	5,50
5	5,50

Table 4.10: Buckling loads for different scaling of imperfections with initial velocity = 0,005m/s

It is seen from table (4.9) and (4.10) that the buckling load is changed when the amplitude of the amplitudes varies. From table (4.10) it can be observed that the buckling load decreases when scaling of higher order buckling modes are large.

When looking at figure (4.18), it is expected that the buckling loads decreases when the amplitudes of imperfections increases. This coincides also with the theory presented by (Weller et al., 1989), see figure (4.20).

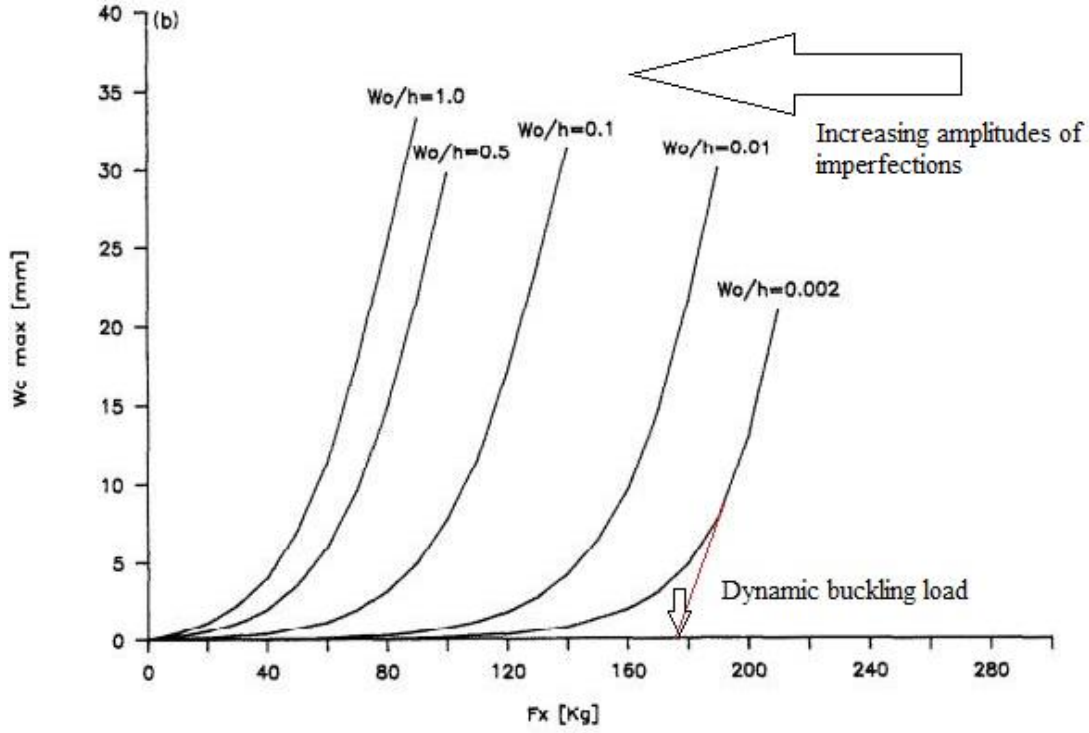

Figure 4.20: Dynamic buckling loads for different values of initial imperfections

From figure (4.20) it is seen that the buckling load decreases when the amplitude of the imperfections are increases, i.e. they are inverse proportional. The results presented in table (4.10) does not coincide with the theory presented by (Weller et al., 1989).

4.6 Analytical results

Analytical results of a simply supported plate (see fig 4.21) can be obtained by following the derivations done by (Ekstrom, 1973). In this section the equations are solved numerically and plotted. This is done by using the computer program *MATLAB*.

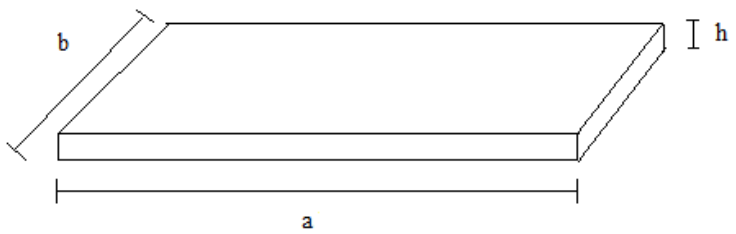

Figure 4.21: Plate

4.6.1 Mathematical procedure

The solution of the equations (Ekstrom, 1973) developed can be found by following the procedure for solution of a 2nd order differential equation, found in (Kreyszig, 2006). Equation (4.2) can be classified as a 2nd order nonlinear differential equation for the plate.

$$\frac{d^2\varsigma}{d\tau^2} + S\left\{\frac{(m^4 + 2R_{12}m^2\beta^2 + R_{22}\beta^4)}{4}(\varsigma - \varsigma_0) + \frac{(1-\upsilon_{xy}\upsilon_{yx})}{8}(m^4 + R_{22}\beta^4)(\varsigma^2 - \varsigma_0^2)\varsigma - m^2\tau\varsigma)\right\} = 0 \quad (4.2)$$

where *m* are the number of halfwaves in the imperfection shape. The following are defined to be able to solve equation (4.2).

$$p_1 = \frac{4D_x\pi^2}{a^2h} \quad (4.3)$$

$$\varsigma = \frac{f}{h} \quad (4.4)$$

$$\varsigma_0 = \frac{f_0}{h} \quad (4.5)$$

f and f_0 are the values of the imperfections of the plate. Further, the following is defined

$$\beta = \frac{a}{b} \quad (4.6)$$

where β is the aspect ratio of the plate.

$$\tau = \frac{p}{p_1} = \frac{ct}{p_1} \quad (4.7)$$

From equation (4.7) it is seen that the average compressive stress increases linearly with time, i.e. $p = ct$. The Greek letter τ is used as the non-dimensional time, and this parameter is used later in this section to plot the response curves for a plate. The parameter p_1 is the static critical stress for a simply-supported isotropic square plate of side a and rigidity D_x. Steel is the material of choice, which is an isotropic material, i.e. the material properties are uniform in all directions. To be able to solve equation (4.2) the following equations have to be defined.

$$R_{12} = \frac{D_1 + 2D_{xy}}{D_x} \tag{4.8}$$

$$R_{22} = \frac{D_y}{D_x} = \frac{E_y}{E_x} \tag{4.9}$$

$$S = \frac{p_1^3 g \pi^2}{c^2 a^2 \gamma} \tag{4.10}$$

For isotropic materials the parameters R_{12} and R_{22} in equation (4.8) and (4.9) are defined as $R_{12} = R_{22} = 1$. (Ekstrom, 1973) solved equation (4.2) numerically using a variable step fourth-order *Runge-Kutta* method. In this report the equation is solved using Euler's method, also known as 1st order *Runge-Kutta* method. Since equation (4.2) is a 2nd order differential equation, the problem can be solved by dividing equation (4.2) into two 1st order differential equations. Equation (4.2) can be simplified to equation (4.11).

$$\frac{d^2\varsigma}{d\tau^2} + S\left\{A(\varsigma - \varsigma_0) + B(\varsigma^2 - \varsigma_0^2)\varsigma - C\tau\varsigma)\right\} = 0 \tag{4.11}$$

By introducing the following conditions, equation (4.11) can be divided into a system of 1st order differential equations.

$$\begin{aligned} \varsigma_1 &= \varsigma \\ \varsigma_2 &= \varsigma' \end{aligned} \tag{4.12}$$

The system of equations will then be

$$\varsigma_1' = \varsigma_2 \tag{4.13}$$

$$\varsigma_2' = -S\left\{A(\varsigma_1 - \varsigma_0) + B(\varsigma_1^2 - \varsigma_0^2)\varsigma - C\tau\varsigma_1\right\} \tag{4.14}$$

Equations (4.13) and (4.14) form the equation set which can be solved by using *Euler's method* and *MATLAB*.

4.6.2 Results from *MATLAB*

The script programmed in *MATLAB* makes it possible to plot the response curve for different values of the initial imperfections. The shape of the imperfection is equal to one half-wave. It is of interest to compare these results with the results obtained in *ABAQUS* to find the goodness of these results.

First, it is interesting to use a plate with equal dimensions as (Ekstrom, 1973) used to find out it is possible to obtain the same results using *MATLAB*. Figure (4.22) and (4.23) shows the results obtained by (Ekstrom, 1973). Figure (4.22) shows the effect on response curves with the same level of initial imperfections, but with different values of loading rate.

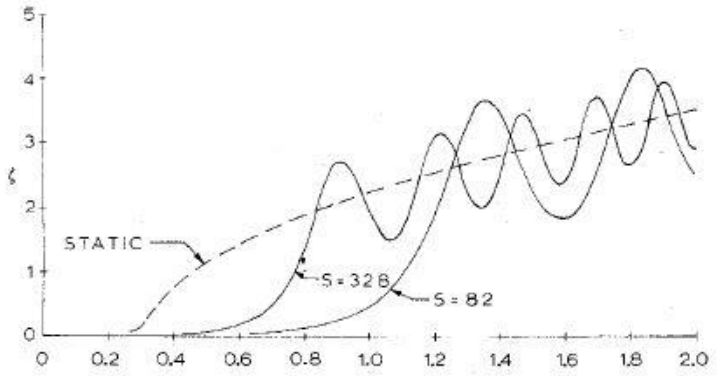

Figure 4.22: Response curve for initial imperfections, ζ_0 = 0.01, different loading rates

Figure (4.23) shows the effect on different values of initial imperfections, when the loading rate is kept constant.

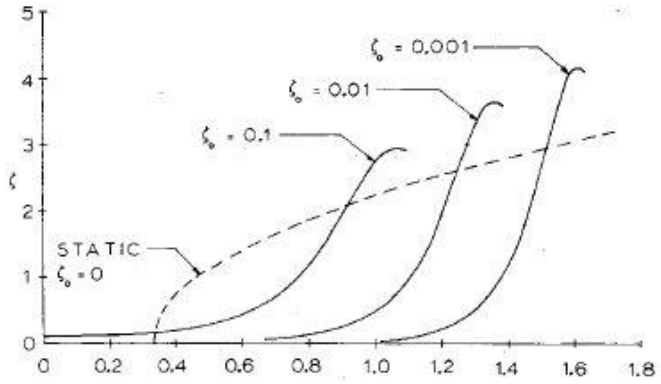

Figure 4.23: Response curve for plates with equal loading rate

When using the material data obtained from (Ekstrom, 1973) and using *Runge-Kutta* 1st order in *MATLAB*, the following results are obtained, see figure (4.24).

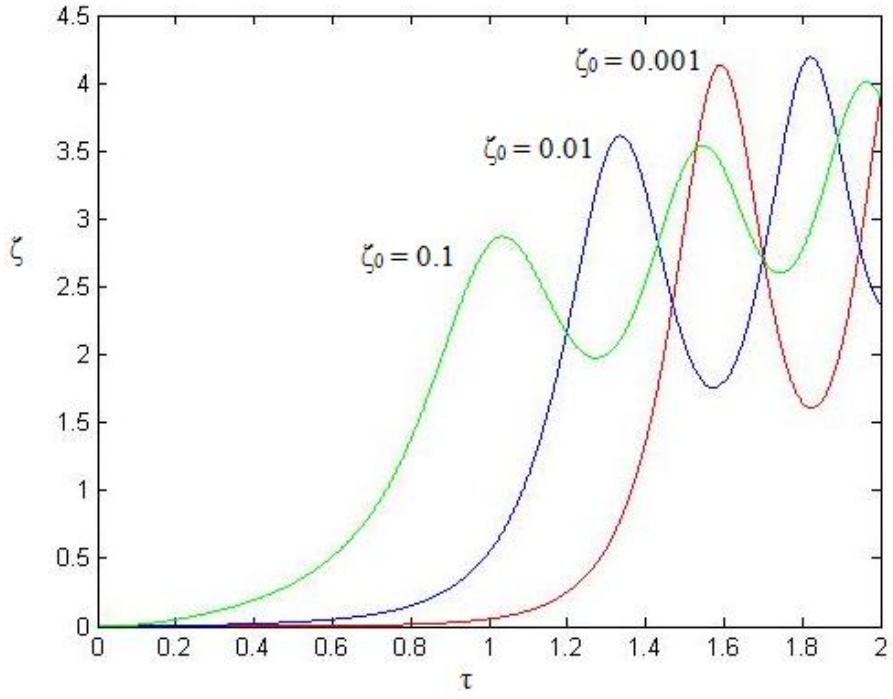

Figure 4.24: Response curve calculated from *MATLAB* with equal loading rate

By comparing the curves in figure (4.22) and (4.23) with figure (4.24), it is observed that good correspondence is obtained between results from (Ekstrom, 1973) and *MATLAB.*

The next step is to perform analyses in *ABAQUS* on a plate with equal dimensions as the plate used in (Ekstrom, 1973), but by using steel as the material of choice. The analysis is performed in the same way as in section 4.3, i.e. by using an edge load with an initial velocity. The load is modelled as a triangular pulse. The buckling mode for initial imperfection, ζ_0 = 0.1, is shown in figure (4.25) and (4.26).

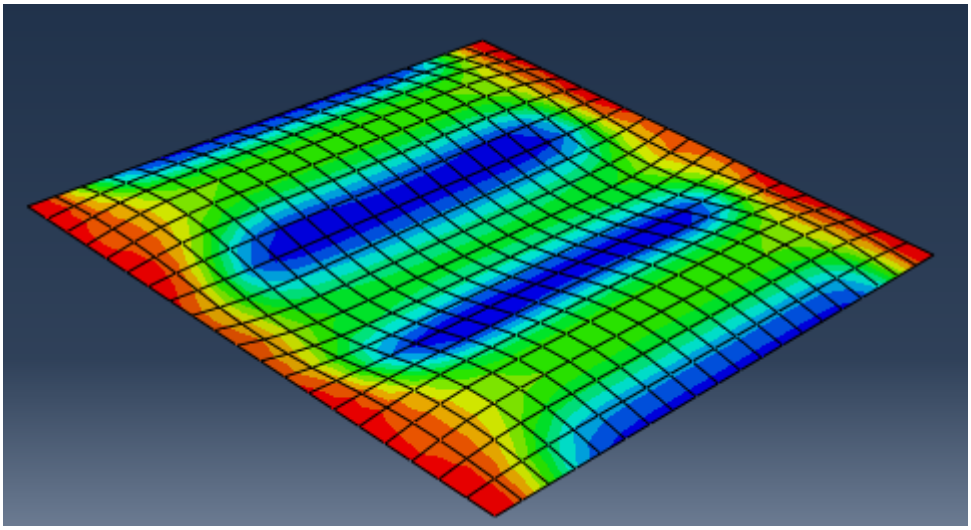

Figure 4.25: Buckling mode, initial velocity = 0.01m/s, t = 10mm

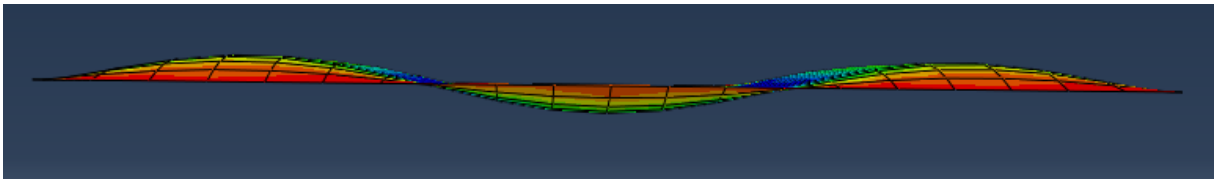

Figure 4.26: Buckling mode, initial velocity = 0.01 m/s, t = 10mm

The material data from the plate analyzed in *ABAQUS* can be used in equation (4.2) and by using the same *MATLAB*-program as used earlier, the following results are obtained, see figure (4.27).

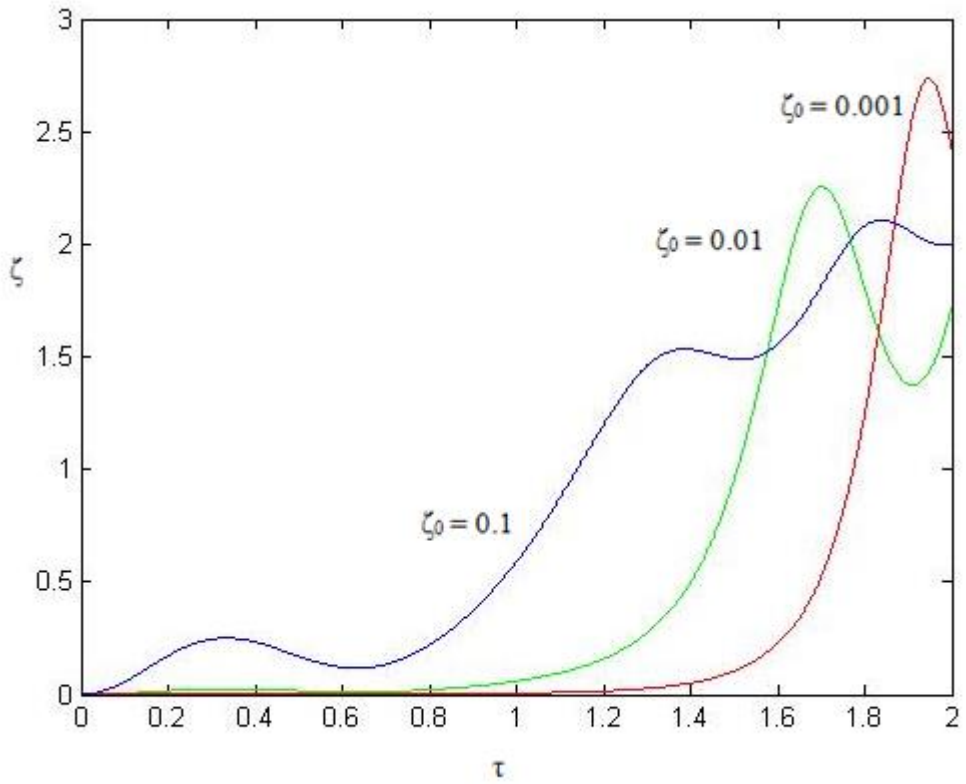

Figure 4.27: Response curve: Velocity of impacting load = 0.01 m/s and equal loading rate

The results from *ABAQUS* are shown in figure (4.28) to figure (4.30).

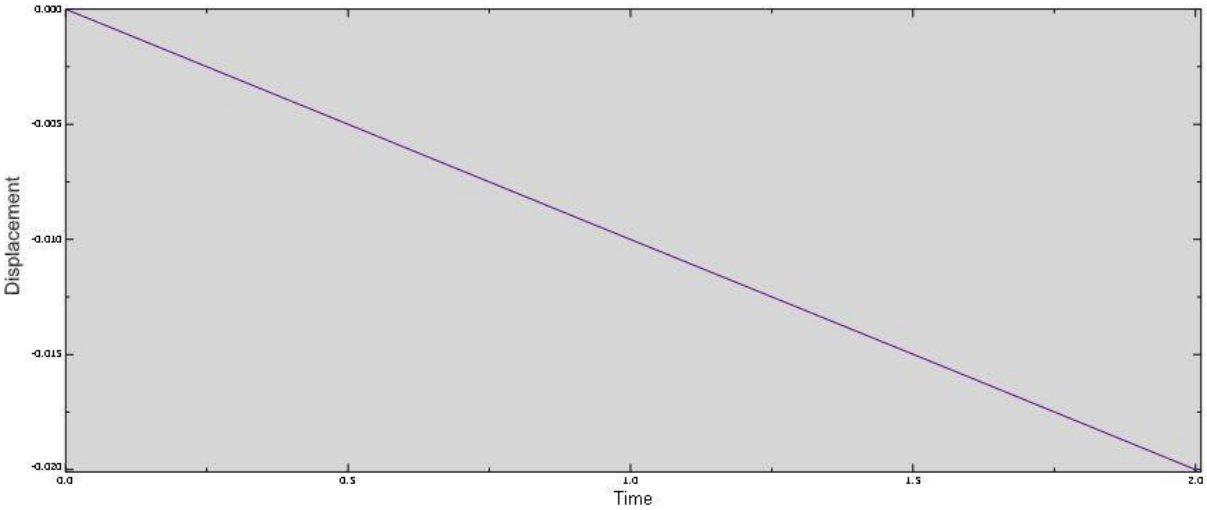

Figure 4.28: Response curve over time history, velocity of impacting load = 0.01 m/s, imperfection $\zeta_0 = 0.1$

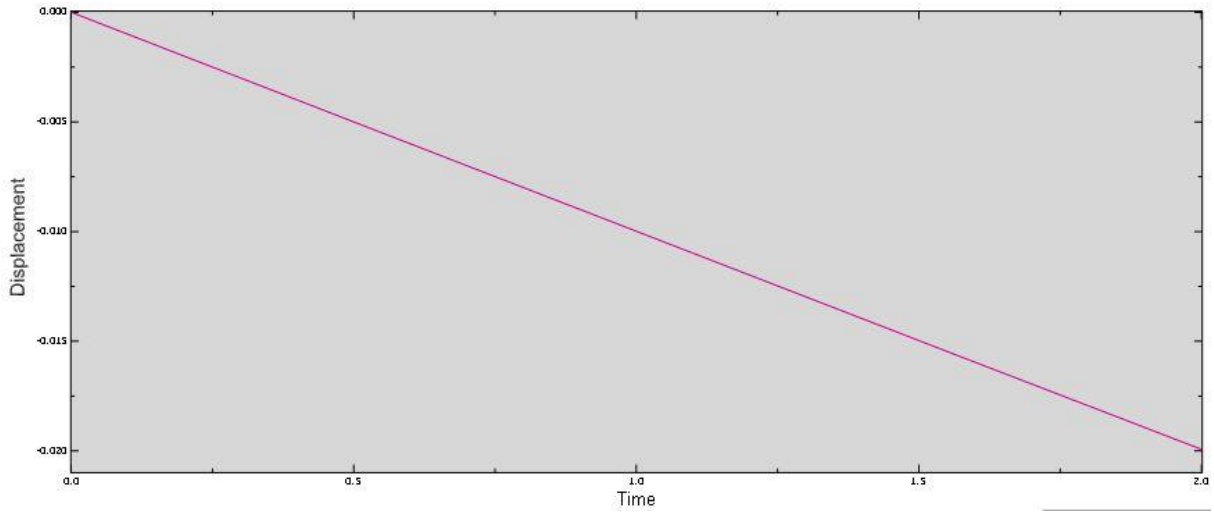

Figure 4.29: Response curve over time history, velocity of impacting load = 0.01 m/s, imperfection ζ_0 = 0.01

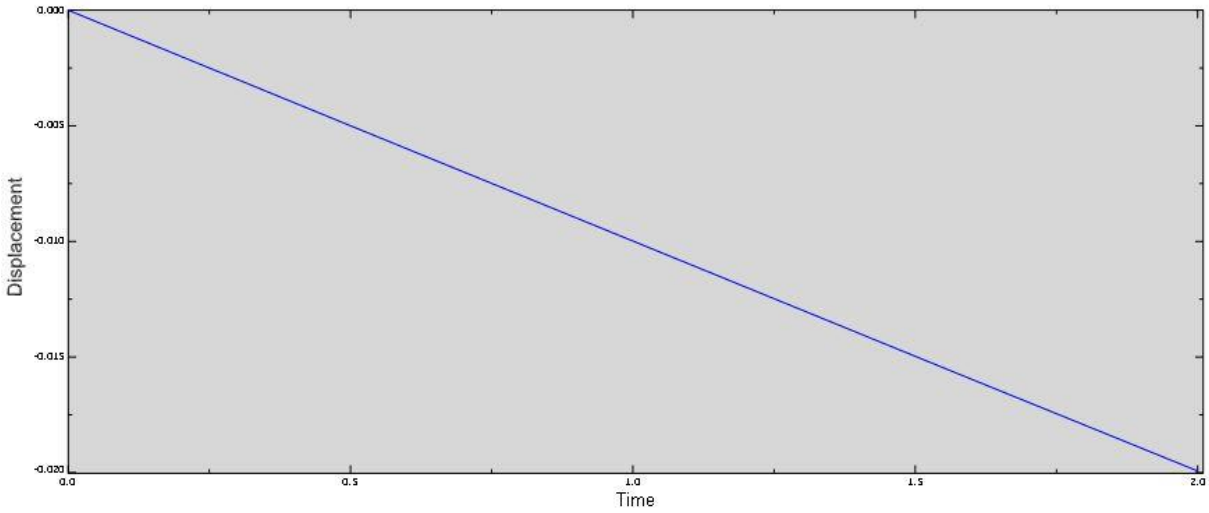

Figure 4.30: Response curve over time history, velocity of impacting load = 0.01 m/s, imperfection ζ_0 = 0.001

The results obtained in *ABAQUS* indicate that the response curve is independent on the level of initial imperfections. This is not in correspondence with the results obtained by (Ekstrom, 1973).

4.7 Analyses with realistic values of yield stress

To keep the plate out of its plastic zone the analyses run in chapter 4 has been performed by using an unrealistic high value for the yield strength. As for the column investigated in chapter 3, it is of interest to run some of the analysis in chapter 4 with a realistic yield strength.

Eigenmodes up to the 4th order (5 half-waves) are implemented as initial imperfections. The yield strength is set to 240MPa and the velocity of the impacting load is set to 0.1m/s. By running the analyses the effect of yielding on the dynamic buckling loads are investigated. Results are tabulated in table (4.11).

Reduced slenderness [-]	**Buckling load with σ_y = 240MPa [kN]**	**Buckling load with σ_y = 240E+10MPa**
3,45	26	26
2,30	89	90
1,73	190	200

Table 4.11: Buckling loads on plates with varying reduced slenderness

It is seen from table (4.11) that the buckling loads do not change much when a realistic yield strength is used. Although the buckling loads are equal the time history of the reaction forces are highly different. Figure (4.31) and (4.32) shows the time history of the reaction force for the realistic case and unrealistic case, respectively.

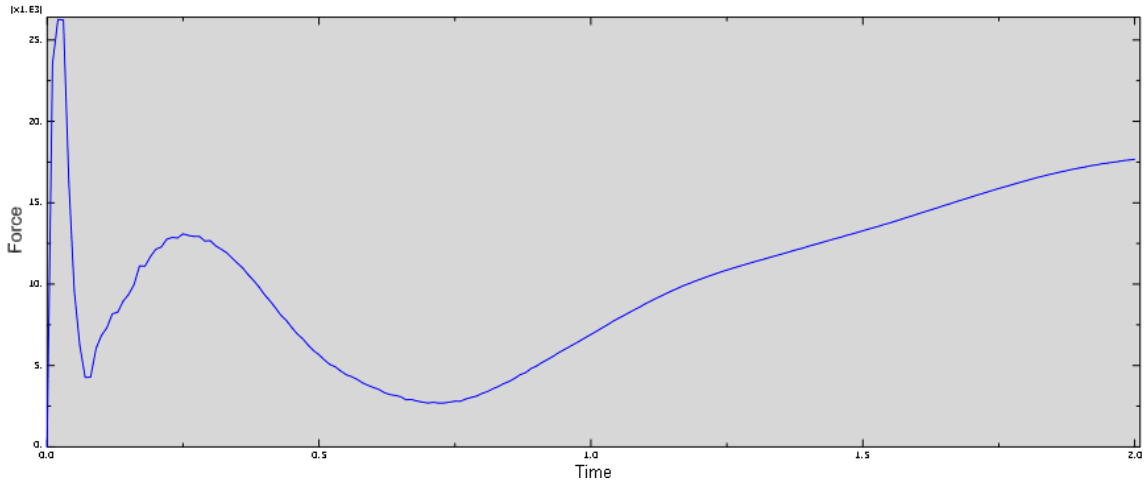

Figure 4.31: Time history for of the reaction force, realistic yield strength

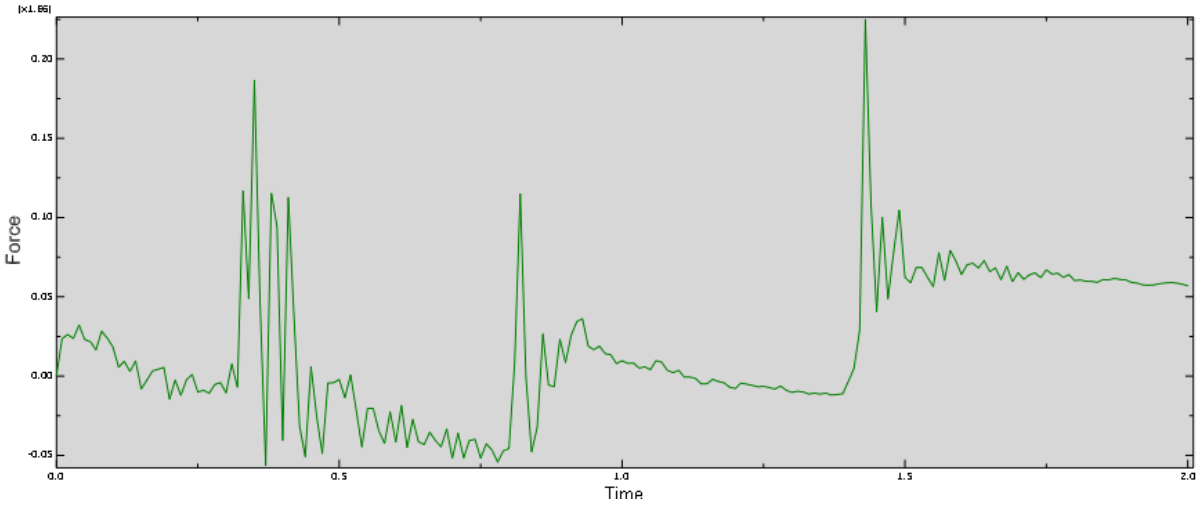

Figure 4.32: Time history of the reaction force, high yield strength

The deformation pattern of the plate will however change. Figure (4.33) to (4.35) shows the difference in buckling pattern when a realistic yield strength is introduced. It is seen from the figures that areas with high *von Mises* stresses are experienced when the yield strength is decreased. The magnitudes of the maximum values are in the vicinity of the yield strength.

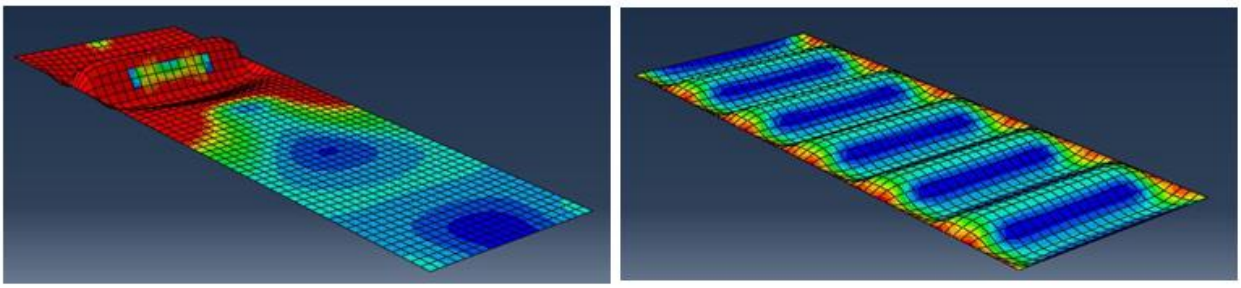

Figure 4.33: Comparison of deformation pattern, realistic yield strength shown on left side, t = 10mm

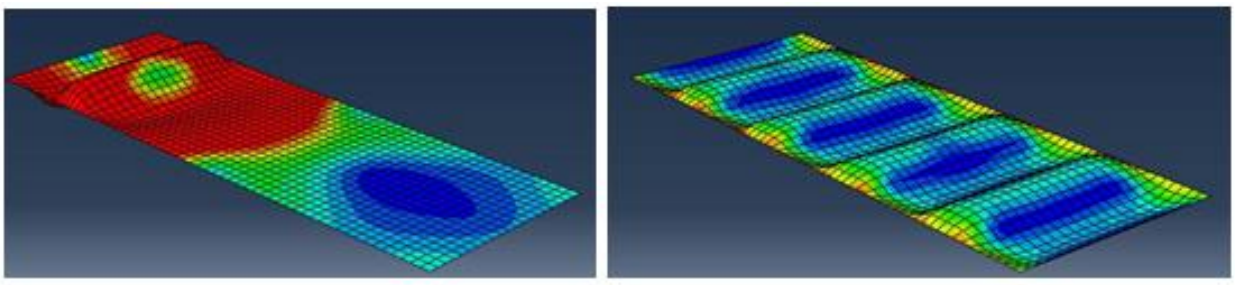

Figure 4.34: Comparison of deformation pattern, realistic yield strength shown on left side, t = 15mm

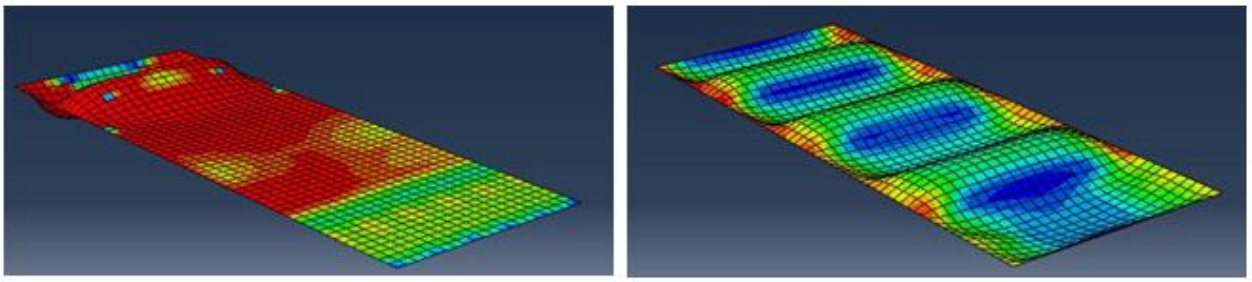

Figure 4.35: Comparison of deformation pattern, realistic yield strength shown on left side, t = 20mm

4.8 Discussion

The results from chapter 4 indicate that, as for columns, the dynamic buckling load *increases* when the slenderness of the plate is *decreased*. This was also confirmed by theory conducted by (Cui et al., 2002). It was also experienced that the impacting velocity of the edge load affected the dynamic buckling loads and the buckling modes of the plate. By investigating the transition velocity between the different buckling modes, it was found that the 4th order buckling mode (5 half-waves) was excited at low impacting velocities. This was different compared to the columns analyzed in chapter 3 where the impacting velocity had to be significantly increased to elicit the highest order buckling mode.

It was observed that by increasing the impacting velocity to 0.05 m/s it was possible to elicit buckling modes with both 8 and 9 half-waves, even though the highest buckling mode implemented only contained 5 half-waves. By gradually implementing buckling modes of higher order it was experienced that the dynamic buckling load decreased. This tendency was valid up to the 4th order buckling mode. As higher order buckling modes were implemented, the dynamic buckling load was constant. The results also indicated that scaling of the combinations of the eigenmodes affected the buckling loads

The analyses with different combinations of eigenmodes showed that the scaling of the eigenmodes had a significant effect on the buckling loads. Results presented in figure (4.18) give reason to assume that imperfections with large amplitudes lead to low buckling loads. This assumption is further investigated in section 4.5.2, were analyses with different scaling of eigenmodes are performed. From table (4.9) and (4.10) it is however observed that the assumption is not necessarily valid. Results indicate that scaling higher order buckling modes large compared to lower order buckling modes, will lead to a decrease in the dynamic buckling load. This is shown in combination 1 and 5 in table (4.12). The maximum amplitudes of the imperfections are equal, but the buckling load for combination 1 is over twice as large as the buckling load for combination 5. The combinations consist of the same eigenmodes, but in combination 5 the higher order buckling modes are scaled larger than the lower order buckling modes. From earlier it would be natural to assume that the buckling

loads would be in vicinity of each other, but as table (4.12) shows, the difference is fairly large. This indicates that scaling of the different eigenmodes is an important parameter to take into account when dealing with analysis of dynamic buckling.

Combination of scaling	**Amplitude [mm]**				**Maximum amplitude [mm]**	**Buckling load [kN]**
	Eigenmode 1 2 half-waves	Eigenmode 2 3 half-waves	Eigenmode 3 4-halfwaves	Eigenmode 4 5 half-waves		
1	3	2	1	0,5	6,5	12,35
5	0,5	1	2	3	6,5	5,50

Table 4.12: Buckling loads for different scaling of eigenmodes

The analytical results showed that the program constructed in *MATLAB* was able to produce the same results as (Ekstrom, 1973). The results from *ABAQUS* are however not in correspondence with the results presented by (Ekstrom, 1973). The results obtained in *ABAQUS* indicate that the response curve is independent on the level of initial imperfections. This is clearly wrong when looking at the results from (Ekstrom, 1973) and analyses performed earlier. The dependence on level of imperfections was shown in table (4.10) where different scaling and combinations of imperfections resulted in different buckling loads and patterns. From theory it is expected that the response curve will be zero until the critical load is reached. This critical load is also known to be sensitive to initial imperfections in the plate. After this load is reached, non-zero deflections are possible and the load-deflection relation is a second-order parabola (Ekstrom, 1973). Since the figures obtained from *ABAQUS* are straight lines, this strengthens the statement that these results are wrong.

There can be many factors that result in wrong results obtained in *ABAQUS.* One obvious source of error is the setup of the analysis. The plate is modelled as simply-supported, and the edges of the plate are set to remain straight during deformation. This is in agreement with (Ekstrom, 1973). The modelling of imperfections by using eigenvalues is also correct. The assumption that the load is modelled as an edge load with an initial velocity, can be questioned when considering the approach of (Ekstrom, 1973). Since the effect of loading rate is investigated, a better way to model the load may have been to use a controlled rate of edge displacement. Since it is not clear which method (Ekstrom, 1973) used, this could be the

reason for the wrong results. A solution to the problem may then be to change the loading from a controlled rate of force increase to a controlled rate of relative edge displacement.

The results from the analyses with a realistic value for the yield strength indicate that the buckling loads are independent on yield strength. This do not coincide with the analyses done for the beam-column in chapter 3, where the buckling loads were significantly reduced. The deformation pattern and reaction forces for the two cases are however completely different. In advance it would have been expected that the deformation patterns for the case where the realistic value is used would have been opposite of the ones obtained from *ABAQUS*, i.e. that maximum deflection is observed near the loaded edge. This can be demonstrated by the deformation of a hood of a car after a car crash, see figure (4.36). From the figure it is observed that the deflection of the hood is largest near the place of impact, see figure (4.36) (safety", 2006). This is also confirmed by (Lindberg, 2003); Buckling is concentrated near the impacted end because the axial load is experienced for the longest time at this location.

Figure 4.36: Deflection from car crash

The reason for the difference can be the modelling of the boundary conditions of the plate. It has been found out that different boundary conditions will induce different plastic collapse mechanisms of plates (Kiat Cheong et al., 2000). The loaded edge is free to move inwards, but the opposite side is fixed from all translations. A hypothesis for the shape of the deflection pattern can be; the deformation pattern is related by the stress waves that occur in the plate when the edge load hits the plate. As the edge load hits the plate a stress wave will start to propagate towards the opposite edge. The stress wave will be reflected and interact with the oncoming stress wave. This will lead to a deformation on the edge parallel to the loaded edge.

5 Further work

For further work it would be interesting to expand the analysis to investigate the effect of a static utilization prior to application of the dynamic force. This situation can be highly relevant in real life. Components in structures are often subjected to a static force, and it is of

interest to investigate how this affects the dynamic buckling load of the component. These components can be columns in a leg of an offshore platform, or plates in the hull of a ship. The columns are for example subjected to a static force from the deck of the platform. If there is a collision between a platform and a ship, dynamic buckling can occur. It could also be interesting to expand the analysis to look at several columns and plates (panels), and how they interact with respect to dynamic buckling.

The investigation between the theoretical results obtained in (Ekstrom, 1973) and analyses performed in *ABAQUS* should also be further analyzed. This is also the case for the analyses where the realistic yield strength is used. The results from both the column and plate were questionable, and further analyses on this subject are recommended.

It would also be interesting to perform real-life experiments with plates, both unstiffened and stiffened. By using high-speed digital cameras, the development of deformation pattern can be determined. This was done by (Featherston et al., 2010), but with focus on the relationship between dynamic and static buckling loads. A natural next step is to expand the analysis to look at dynamic buckling on stiffened panels on ships or platforms. This will give further insight into the phenomenon *dynamic buckling.*

6 Conclusion

The main focus in this thesis has been to investigate parameters that affect dynamic buckling. It has been found that there are several parameters that have influence on the dynamic buckling loads. The reduced slenderness of a plate or column will have a major influence on the dynamic buckling loads. When performing analyses scaling of imperfections should also be handled with care. An *increase* in both magnitude of imperfections and reduced slenderness will lead to a significant *reduction* in dynamic buckling loads.

The modelling of initial imperfections by using the columns/plates eigenmodes works well. The dynamic buckling load is however unaffected when adding buckling modes of high order. Buckling modes of 3^{rd} (columns) and 4^{th} (plates) order have shown to be the highest modes necessary to implement. It is possible for a plate to buckle in high order buckling modes which are *not* implemented in the model.

The scaling of the different buckling modes in the model should be performed with caution. Small maximum amplitudes of the imperfections will not necessarily lead to large dynamic buckling loads. The scaling of the different eigenmodes should therefore be taken with care.

It is also important to verify that the loading duration is not close to the natural period of the component. The dynamic loading factor may drop below unity for loading durations in the vicinity of the components natural period.

Since the results when using realistic yield strength values were questionable, the results from this part should be read with caution.

7 References

AMDAHL, J. 2009. Chapter 3: Buckling of stiffened plates. *TMR4205, Buckling and ultimate strength of marine structures*.

ARI-GUR, J., WELLER, T. & SINGER, J. 1982. Experimental and theoretical studies of columns under axial impact. *International Journal of Solids and Structures,* 18**,** 619-641.

ARI-GUR, J. S., J; WELLER, T 1981. Dynamic buckling of plates under longitudinal impact. *Israel journal of technology*

19**,** 57-64.

ARI GUR, J. & WELLER, T. 1985. EXPERIMENTAL STUDIES WITH METAL PLATES SUBJECTED TO INPLANE AXIAL IMPACT.

BUDIANSKY, B. & HUTCHINSON, J. W. 1964. *Dynamic buckling of imperfection-sensitive structures,* Division of Engineering and Applied Physics, Harvard University.

CUI, S., HAO, H. & KIAT CHEONG, H. 2002. Theoretical study of dynamic elastic buckling of columns subjected to intermediate velocity impact loads. *International Journal of Mechanical Sciences,* 44**,** 687-702.

CUI, S., KIAT CHEONG, H. & HAO, H. 1999. Experimental study of dynamic buckling of plates under fluid-solid slamming. *International Journal of Impact Engineering,* 22**,** 675-691.

EKSTROM, R. E. 1973. Dynamic buckling of a rectangular orthotropic plate. *AIAA* 11**,** 1655-1659.

FEATHERSTON, C. A., MORTIMER, J., EATON, M., BURGUETE, R. L. & JOHNS, R. 2010. The dynamic buckling of stiffened panels - A study using high speed digital image correlation. *Applied Mechanics and Materials.* Liverpool.

JI, W. & WAAS, A. M. 2013. The temporal evolution of buckling in a dynamically impacted column. *Journal of Applied Mechanics, Transactions ASME,* 80.

KIAT CHEONG, H., HAO, H. & CUI, S. 2000. Experimental investigation of dynamic post-buckling characteristics of rectangular plates under fluid-solid slamming. *Engineering Structures,* 22**,** 947-960.

KREYSZIG, E. 2006. Advanced Engineering Mathematics, Mathematica Computer Guide. *Chapter 4.5: Qualitative methods for nonlinear systems*.

LANDA, A. 2013. The buckling resistance of structures subjected to impulsive type actions.

LINDBERG, H. E. 2003. Little book of dynamic buckling.

LINDBERG, H. E. & FLORENCE, A. L. 1987. Dynamic pulse buckling - Theory and experiment.

MA, G., LIU, Y. & LI, Q. 2006. Numerical simulations of dynamic instability of elastic-plastic beams. *Journal of Engineering Mechanics,* 132**,** 260-267.

MATHISEN, K. M. 2011. TMR4190, Elementmetoden anvendt i konstruksjonsanalyse, lecture 14.

PIAN, T. H. H. & SIDDAL, J. N. 1950. Navy report. *Mass. Inst. Tech.*

SAFETY", I. I. F. H. 2006. Crash test: 2006 Hyundai Tuscon GLS 4wd.

WELLER, T., ABRAMOVICH, H. & YAFFE, R. 1989. Dynamic buckling of beams and plates subjected to axial impact. *Computers & Structures,* 32**,** 835-851.

8 Appendix

The appendix contains the most important model and control files from *USFOS* and the keywords from the analysis done in *ABAQUS*. Complete program files are attached to the thesis via a zip-file.

8.1 Dynamic analysis with column with length = 10m

The transition velocity between the different buckling modes is found by changing the parameter Vx under INI_VELO.

8.1.1 Control file

```
'              Dynamic analysis: Nodeload with initial velocity
'                      Created by: Andreas Landa
'                       NTNU, Trondheim
HEAD
'EIGENVAL   Time          0.1                ! Perform eigenval at time = 1
'EIGENVAL   NumberOf      40                 ! Compute 20 vectors
'EIGENVAL   Algorithm     Lanczos            ! Use Lanczos solver
'EIGENVAL   ModeScale      20                 ! Scale modes by  2OPor visualization
'EIGENVAL   Shift         -0.1
'                  End_time   delta_t   dT_res   dT_term
DYNAMIC            0.10         0.001     0.001    0.001
'          ID     Type
TIMEHIST    1  Points
'         Time   Factr
             0.0     .0
              1.0    1.0
'            Load_case    time_histID
LOADHIST   1            1
'          Type Time      Vx        Vy   Vz  rVx  rVy  rVz  Id
INI_VELO   Node   0.0     0.2/1.0    0    0     0      0         0   1
'          ncnodes
CNODES     1
'          nodex  idof  dfact
```

```
           1      1     1.
'                  Type    Elem_ID  End  Dof
DYNRES_E   Force          4           1      X
'                   Rat1    Rat2    Freq1    Freq2
DAMPRATIO  0.01    0.01     0.1      10.0
```

8.1.2 Model file

```
'              Dynamic analysis: Nodeload with initial velocity
'                     Created by: Andreas Landa
'                         NTNU, Trondheim'
'            Node ID          X          Y         Z          Boundary code
 NODE          1            .000     .000          .000         0 1 1 1 0 1
 NODE          2           2.500     .000          .0011665     0 1 0 1 0 1
 NODE          3           5.000     .000         .000667       0 1 0 1 0 1
 NODE          4           7.500      .000        .0001665      0 1 0 1 0 1
 NODE          5          10.000     .000         .000          1 1 1 1 0 1
'
'            Elem ID      np1       np2    material    geom
 BEAM              1       1         2         1         1
 BEAM              2       2         3         1         1
 BEAM               3      3         4         1         1
 BEAM              4       4         5         1         1

'            Geom ID        Do          Thick
PIPE             1         .24070       .00500
'            ID     Mass
NODEMASS     1      1.0E+10

'          matno    E-mod         poiss     yield             density     term.exp
MISOIEP    1       210000.0E+6    0.3      240.0E+16          7850     1.4E-05
'            Load case     Acc_X    Acc_Y       Acc_Z
GRAVITY             1      0        0     -9.81
```

8.2 Dynamic analysis with column with length = 15m

The transition velocity between the different buckling modes is found by changing the parameter Vx under INI_VELO.

8.2.1 Control file

```
'              Dynamic analysis: Nodeload with initial velocity
'                      Created by: Andreas Landa
'                   NTNU, Trondheim
HEAD
'                    restart result print
CSAVE              0       1      0
'          ncnodes
CNODES     1
'          nodex  idof  dfact
           1      1     1.


'EIGENVAL   Time          1.0                ! Perform eigenval at time = 1
'EIGENVAL   NumberOf      20                 ! Compute 20 vectors
'EIGENVAL   Algorithm     Lanczos            ! Use Lanczos solver
'EIGENVAL   ModeScale      2                 ! Scale modes by  2Por visualization
'EIGENVAL   Shift        -0.1


'                   End_time   delta_t   dT_res   dT_term
DYNAMIC    0.2          0.001     0.001    0.001
'          ID     Type
TIMEHIST    1  Points
'         Time   Factr
           0.0     .0
           0.1    1.0
           1.0    1.0
'         Load_case    time_histID
LOADHIST   1            1
```

```
'            Type     Time       Vx           Vy    Vz   rVx   rVy   rVz   Id
INI_VELO      Node          0.0    0.2/1.0      0       0     0       0        0   1

'                   Type          Elem_ID  End   Dof
DYNRES_E    Force  4       1       X

'                    Rat1    Rat2    Freq1    Freq2
DAMPRATIO  0.01    0.01     0.1      10.0
```

8.2.2 Model file

```
'              Dynamic analysis: Nodeload with initial velocity
'                       Created by: Andreas Landa
'                           NTNU, Trondheim'
'            Node ID        X           Y            Z            Boundary code
 NODE        1              .000       .000          .000         0 1 1 1 0 1
 NODE        2             3.750       .000          .0175        0 1 0 1 0 1
 NODE        3             7.500      .000           .0100        0 1 0 1 0 1
 NODE        4             11.250      .000          .0025        0 1 0 1 0 1
 NODE        5             15.000      .000          .000         1 1 1 1 0 1
'
'            Elem ID     np1       np2    material    geom
 BEAM              1             1         2         1         1
 BEAM              2             2         3         1         1
 BEAM               3            3         4         1         1
 BEAM              4             4         5         1         1
'            Geom ID        Do          Thick
 PIPE             1         .24070       .00500
'            ID     Mass
NODEMASS     1      1.0E+10
```

```
'                   matno    E-mod              poiss    yield       density
term.exp
MISOIEP     1        210000.0E+6  0.3      240.0E+16          7850         1.4E-05


'            Load case   Acc_X    Acc_Y    Acc_Z
GRAVITY              1      0        0           -9.81
```

8.3 Dynamic analysis with column with length = 20m

The transition velocity between the different buckling modes is found by changing the parameter Vx under INI_VELO.

8.3.1 Control file

```
'              Dynamic analysis: Nodeload with initial velocity
'                      Created by: Andreas Landa
'                    NTNU, Trondheim
HEAD
'EIGENVAL    Time            0.1                      ! Perform eigenval at time = 1
'EIGENVAL    NumberOf       40                        ! Compute 20 vectors
'EIGENVAL    Algorithm      Lanczos                   ! Use Lanczos solver
'EIGENVAL    ModeScale       20                       ! Scale modes by  2OPor
visualization
'EIGENVAL    Shift          -0.1
'                     End_time        delta_t        dT_res          dT_term
DYNAMIC              0.2          0.00001     0.00001     0.00001
'                     ID     Type
TIMEHIST     1   Points
'          Time    Factr
             0.0      .0
             0.1     1.0
             1.0     1.0
'          Load_case     time_histID
LOADHIST    1             1


'             Type     Time       Vx        Vy    Vz   rVx   rVy   rVz   Id
```

```
INI_VELO   Node       0.0      0.2/1.0     0     0     0       0         0      1
'          ncnodes
CNODES     1
'          nodex  idof  dfact
           1      1     1.
'                  Type    Elem_ID  End  Dof
DYNRES_E   Force           4        1    X
'                  Rat1    Rat2    Freq1    Freq2
DAMPRATIO  0.01    0.01     0.1      10.0
```

8.3.2 Model file

```
'              Dynamic analysis: Nodeload with initial velocity
'                     Created by: Andreas Landa
'                       NTNU, Trondheim'
'            Node ID    X              Y              Z           Boundary code
 NODE        1       .000              .000              .000         0 1 1 1 0 1
 NODE        2      5.000              .000              .0233        0 1 0 1 0 1
 NODE        3     10.000              .000              .0133        0 1 0 1 0 1
 NODE        4     15.000              .000              .0033        0 1 0 1 0 1
 NODE        5      20.000             .000              .000         1 1 1 1 0 1

'
'            Elem ID     np1       np2    material    geom
 BEAM              1            1        2        1        1
 BEAM              2            2        3        1        1
 BEAM              3            3        4        1        1
 BEAM              4            4        5        1        1
'            Geom ID       Do          Thick
 PIPE              1        .24070      .00500
'            ID     Mass
NODEMASS    1      1.0E+10
```

```
'                   matno    E-mod              poiss    yield       density
term.exp
MISOIEP     1         210000.0E+6  0.3      240.0E+16          7850         1.4E-05
'         Load case   Acc_X    Acc_Y    Acc_Z
GRAVITY               1       0        0      -9.81
```

8.4 Dynamic analysis: Investigation of magnitude of imperfection

To investigate the effect of magnitude of imperfection, the change was done in the model file. The code under shows the procedure for the column with length equal to 10m.

8.4.1 L / 1000

```
'             Node ID       X           Y           Z           Boundary code
 NODE            1          .000        .000        .000        0 1 1 1 0 1
 NODE            2          2.500       .000        .0011665    0 1 0 1 0 1
 NODE            3          5.000       .000        .000667     0 1 0 1 0 1
 NODE            4          7.500       .000         .0001665   0 1 0 1 0 1
 NODE            5         10.000        .000        .000        1 1 1 1 0 1
```

8.4.2 L /100

```
'             Node ID       X           Y           Z           Boundary code
 NODE            1          .000        .000        .000        0 1 1 1 0 1
 NODE            2          2.500       .000        .011665     0 1 0 1 0 1
 NODE            3          5.000       .000        .00667      0 1 0 1 0 1
 NODE            4          7.500       .000        .001665     0 1 0 1 0 1
 NODE            5         10.000        .000        .000        1 1 1 1 0 1
```

8.4.3 L / 10

```
'             Node ID       X           Y           Z           Boundary code
 NODE            1          .000        .000        .000        0 1 1 1 0 1
 NODE            2          2.500       .000        .11665      0 1 0 1 0 1
 NODE            3          5.000       .000        .0667       0 1 0 1 0 1
 NODE            4          7.500       .000         .01665     0 1 0 1 0 1
 NODE            5         10.000        .000        .000        1 1 1 1 0 1
```

8.5 Effect of yielding

The effect of yielding was investigated by changing the MISOIEP-command in the model file. The command was changed from:

```
'                   matno        E-mod          poiss    yield       density    term.exp
MISOIEP             1            210000.0E+6    0.3      240.0E+16   7850       1.4E-05
to:
'                   matno        E-mod          poiss    yield       density    term.exp
MISOIEP             1            2.1E+5         0.3      240.0       7850        1.4E-05
```

8.6 Eigenvalue analysis in ABAQUS for mesh size = 50mm

```
*Heading
** Job name: Stat_buckl005 Model name: Model-1
** Generated by: Abaqus/CAE 6.12-1
*Preprint, echo=NO, model=NO, history=NO, contact=NO
**
** PARTS
**
*Part, name=Part-1
*Node
      1,           0.,           0.,           1.
      2, 0.0500000007,           0.,           1.
      3,  0.100000001,           0.,           1.
…
*Element, type=S4R
   1,    1,    2,   63,   62
   2,    2,    3,   64,   63
…
*Nset, nset=_PickedSet2, internal, generate
    1,  1281,     1
*Elset, elset=_PickedSet2, internal, generate
    1,  1200,     1
*Nset, nset=_PickedSet3, internal, generate
```

```
    1,  1281,     1
*Elset, elset=_PickedSet3, internal, generate
    1,  1200,     1
** Section: Plate
*Shell Section, elset=_PickedSet2, material=Steel
0.01, 5
*End Part
**
**
** ASSEMBLY
**
*Assembly, name=Assembly
**
*Instance, name=Part-1-1, part=Part-1
*End Instance
**
*Nset, nset=_PickedSet5, internal, instance=Part-1-1, generate
    1,  1221,    61
*Elset, elset=_PickedSet5, internal, instance=Part-1-1, generate
    1,  1141,    60
*Nset, nset=_PickedSet6, internal, instance=Part-1-1
    1,    2,    3,    4,    5,    6,    7,    8,    9,   10,   11,   12,   13,   14,
15,   16
   17,   18,   19,   20,   21,   22,   23,   24,   25,   26,   27,   28,   29,   30,
31,   32
   33,   34,   35,   36,   37,   38,   39,   40,   41,   42,   43,   44,   45,   46,
47,   48
   49,   50,   51,   52,   53,   54,   55,   56,   57,   58,   59,   60,   61, 1221,
1222, 1223
 1224, 1225, 1226, 1227, 1228, 1229, 1230, 1231, 1232, 1233, 1234, 1235, 1236, 1237,
1238, 1239
 1240, 1241, 1242, 1243, 1244, 1245, 1246, 1247, 1248, 1249, 1250, 1251, 1252, 1253,
1254, 1255
 1256, 1257, 1258, 1259, 1260, 1261, 1262, 1263, 1264, 1265, 1266, 1267, 1268, 1269,
1270, 1271
```

```
 1272, 1273, 1274, 1275, 1276, 1277, 1278, 1279, 1280, 1281
*Elset, elset=_PickedSet6, internal, instance=Part-1-1
    1,    2,    3,    4,    5,    6,    7,    8,    9,   10,   11,   12,   13,   14,
15,   16
   17,   18,   19,   20,   21,   22,   23,   24,   25,   26,   27,   28,   29,   30,
31,   32
   33,   34,   35,   36,   37,   38,   39,   40,   41,   42,   43,   44,   45,   46,
47,   48
   49,   50,   51,   52,   53,   54,   55,   56,   57,   58,   59,   60, 1141, 1142,
1143, 1144
 1145, 1146, 1147, 1148, 1149, 1150, 1151, 1152, 1153, 1154, 1155, 1156, 1157, 1158,
1159, 1160
 1161, 1162, 1163, 1164, 1165, 1166, 1167, 1168, 1169, 1170, 1171, 1172, 1173, 1174,
1175, 1176
 1177, 1178, 1179, 1180, 1181, 1182, 1183, 1184, 1185, 1186, 1187, 1188, 1189, 1190,
1191, 1192
 1193, 1194, 1195, 1196, 1197, 1198, 1199, 1200
*Nset, nset=_PickedSet7, internal, instance=Part-1-1, generate
   61,  1281,    61
*Elset, elset=_PickedSet7, internal, instance=Part-1-1, generate
   60,  1200,    60
*Elset, elset=__PickedSurf4_E2, internal, instance=Part-1-1, generate
   60,  1200,    60
*Surface, type=ELEMENT, name=_PickedSurf4, internal
__PickedSurf4_E2, E2
*End Assembly
**
** MATERIALS
**
*Material, name=Steel
*Density
7850.,
*Elastic
 2e+11, 0.3
*Plastic
```

```
 4e+08,0.
** ----------------------------------------------------------------
**
** STEP: Stat_buckling
**
*Step, name=Stat_buckling, perturbation
Static buckling of simply supported plate
*Buckle
5, , 10, 30
**
** BOUNDARY CONDITIONS
**
** Name: BC-3 Type: Displacement/Rotation
*Boundary, op=NEW, load case=1
_PickedSet7, 2, 2
_PickedSet7, 3, 3
*Boundary, op=NEW, load case=2
_PickedSet7, 2, 2
_PickedSet7, 3, 3
** Name: Fixed Type: Displacement/Rotation
*Boundary, op=NEW, load case=1
_PickedSet5, 1, 1
_PickedSet5, 2, 2
_PickedSet5, 3, 3
*Boundary, op=NEW, load case=2
_PickedSet5, 1, 1
_PickedSet5, 2, 2
_PickedSet5, 3, 3
** Name: Simply supported Type: Displacement/Rotation
*Boundary, op=NEW, load case=1
_PickedSet6, 2, 2
```

```
_PickedSet6, 3, 3
*Boundary, op=NEW, load case=2
_PickedSet6, 2, 2
_PickedSet6, 3, 3
**
** LOADS
**
** Name: Buckling_load   Type: Shell edge load
*Dsload
_PickedSurf4, EDNOR, 1.
**
** OUTPUT REQUESTS
**
*Restart, write, frequency=0
*Print, solve=NO
**
** FIELD OUTPUT: F-Output-1
**
*Output, field
*EL PRINT, ELSET=_PickedSet5, LAST MODE=10
S,E
*EL PRINT, ELSET=_PickedSet6, LAST MODE=10
S,E
*EL PRINT, ELSET=_PickedSet7, LAST MODE=10
S,E,
*NODE FILE, LAST MODE=10
U,
*End Step
```

8.7 Combinations and scaling of eigenmodes

When investigating the effect of different combinations and scaling of imperfections, the command line IMPERFECTION is edited. The input file gets the eigenmodes from the

eigenvalue analysis named *Stat_buckl005*, and the example under is for the combination were the 8 first eigenmodes are implemented and scaled.

```
*IMPERFECTION, FILE=Stat_buckl005, STEP=1

**Eigenmode, scaling

1, 0.003

2, 0

3, 0.002

4, 0.001

5, 0.0005

6, 0.00025

7, 0.000125

8, 0.0000625

9, 0.00003125
```

8.8 Analytical solution in MATLAB

8.8.1 Verification of results in (Ekstrom, 1973)

```
%%%%%%%%%%%%%%%%%%%%%%%%%%%%%%%%%%%%%%%%%%%%%%%%%%%%%%%%%%%%%%%%%%%%%%%
%       Analytical solution of the plate buckling equation%
%                         Andreas Landa                                 %
%                       Trondheim, 2013                                 %
%%%%%%%%%%%%%%%%%%%%%%%%%%%%%%%%%%%%%%%%%%%%%%%%%%%%%%%%%%%%%%%%%%%%%%%



%Parameters are defined

a = 10;                                          % Length [in]
b = 10;                                        % Width [in]
h = 0.05;                                      % Thickness [in]


m = 1;                                         % Number of half-waves

beta = a/b;                                    % Aspect ratio [-]
g = 386.088582677165;                % Gravitational acceleration
                                               % [in/s^2]

Ex = 40E+6;                                    % Elastic modulus [psi]
Ey = 4E+6;                                     % Elastic modulus [psi]
Gxy = 1.5E+6;                                  % Shear modulus [psi]
vxy = 0.25;                                    % Poissons ratio [-]
vyx = 0.025;                                   % Poissons ratio [-]
ny = 0.0585;                                   % Specific weight[lb/in^3]


Dx = (Ex*h^3)/(12*(1-vxy*vyx));                % Flexural
rigidity [Pa*m^3]

Dy = (Ey*h^3)/(12*(1-vxy*vyx));                % Flexural rigidity [Pa*m^3]
```

```
D1 = (Ex*vyx*h^3)/(12*(1-vxy*vyx));          % Flexural rigidity [Pa*m^3]

Dxy = (Gxy*h^3)/12;                          % Flexural rigidity [Pa*m^3

R12 = 0.09953;
R22 = 0.1;
p1 = 3311;                                   % [psi]
pcr = 1075;                                  % Yield stress

c = 537500;                                  % Axial stress wave velocity [in/s]

ksi_0 = 0.1;                                 % Initial imperfection vs. thickness

S = ((p1^3)*g*pi^2)/((c^2)*(a^2)*ny);        % Dynamic similarity number [-]

%Defining constants used in system of equations

A = (m.^4+2*R12*m.^2*beta.^2+R22*beta.^4)/4;
B = ((1-vxy*vyx)*(m.^4+R22*beta.^4))/8;

dx = 0.001;
X = 0:dx:2;
Y = zeros(length(X));
G = Y;
Y(1) = 0;                                    % y(0)
G(1) = 0;                                    % y'(0)
tic
for i = 2:length(X)                          % RK1 (euler)
    Y(i) = Y(i-1) + dx*G(i-1);
    G(i) = G(i-1) + dx*(-S*((A*(Y(i-1)-ksi_0))+(B*(Y(i-1)^2-ksi_0^2))*Y(i-1)-
m^2*X(i-1)*Y(i-1)));
end
tid = toc;
steprate = i/tid;
disp(['    y(x = ' num2str(2) ') = ' num2str(Y(i))]);
disp(['dy/dx(x = ' num2str(2) ') = ' num2str(G(i))]);
plot(X,Y,'r')
hold on
%plot(X,G,'k')
```

8.8.2 Verification in SI-units

```
%%%%%%%%%%%%%%%%%%%%%%%%%%%%%%%%%%%%%%%%%%%%%%%%%%%%%%%%%%%%%%%%%%%%%%%
%       Analytical solution of the plate buckling equation%
%                         Andreas Landa                                  %
%                       Trondheim, 2013                                  %
%%%%%%%%%%%%%%%%%%%%%%%%%%%%%%%%%%%%%%%%%%%%%%%%%%%%%%%%%%%%%%%%%%%%%%%


%Parameters are defined

a = 0.254;                                   % Length [m]
b = 0.254;                                   % Width [m]
h = 0.00127;                                 % Thickness [m]

m = 1;                                       % Number of half-waves
beta = a/b;                                  % Aspect ratio [-]
g = 9.81;                                    % Gravitational acceleration
                                             % [m/s^2]

Ex = 2.76E+11;                               % Elastic modulus [Pa]

Ey = 2.76E+10;                               % Elastic modulus [Pa]

Gxy = 1.03E+10;                              % Shear modulus [Pa]
```

```
vxy = 0.25;                                % Poissons ratio [-]

vyx = 0.025;                               % Poissons ratio [-]

ny = 15885.333;                            % Specific weight[kg/m^3]

Dx = 2.89E+6;                              % Flexural rigidity [Pa]

Dy = 2.89E+5;                              % Flexural rigidity
[Pa]

D1 = 72257.06;                             % Flexural rigidity
[Pa]

Dxy = 107696.11;                           % Flexural rigidity [Pa]

R12 = 0.09953;
R22 = 0.1;
p1 = 2.28E+7;                              % [Pa]
pcr = 7411864;                             % Yield stress[Pa]

c = 3705932043;                            % Axial stress wave velocity [m/s]
ksi_0 = 0.01;                              % Initial imperfection vs. thickness


S = ((p1^3)*g*pi^2)/((c^2)*(a^2)*ny);       % Dynamic similarity number [-]

%Defining constants used in system of equations

A = (m.^4+2*R12*m.^2*beta.^2+R22*beta.^4)/4;
B = ((1-vxy*vyx)*(m.^4+R22*beta.^4))/8;

dx = 0.001;
X = 0:dx:2;
Y = zeros(length(X));
G = Y;
Y(1) = 0;                                   % y(0)
G(1) = 0;                                   % y'(0)
tic
for i = 2:length(X)                         % RK1 (euler)
    Y(i) = Y(i-1) + dx*G(i-1);
    G(i) = G(i-1) + dx*(-S*((A*(Y(i-1)-ksi_0))+(B*(Y(i-1)^2-ksi_0^2))*Y(i-1)-
m^2*X(i-1)*Y(i-1)));
end
tid = toc;
steprate = i/tid;
disp(['    y(x = ' num2str(2) ') = ' num2str(Y(i))]);
disp(['dy/dx(x = ' num2str(2) ') = ' num2str(G(i))]);
plot(X,Y,'r')
```

8.8.3 *MATLAB*-script on plate with dimensions 1x1m

```
%%%%%%%%%%%%%%%%%%%%%%%%%%%%%%%%%%%%%%%%%%%%%%%%%%%%%%%%%%%%%%%%%%%%%%%
%       Analytical solution of the plate buckling equation%
%                         Andreas Landa                                  %
%                       Trondheim, 2013                                  %
%%%%%%%%%%%%%%%%%%%%%%%%%%%%%%%%%%%%%%%%%%%%%%%%%%%%%%%%%%%%%%%%%%%%%%%


%Parameters are defined%

a = 1;                                      % Length [m]
b = 1;                                      % Width [m]
h = 0.01;                                   % Thickness [m]
v = 0.01;                                   % Veloctiy of impacting load
ro = 7850;
```

```
m = 1;                                          % Number of halfwaves in
                                                % imperfection function
beta = a/b;                                     % Aspect ratio [-]
g = 9.81;                                       % Gravitational acceleration
                                                % [m/s^2]

Ex = 2.1E+11;                                   % Elastic modulus [Pa]
Ey = 2.1E+11;                                   % Elastic modulus [Pa]
Gxy = 8.08E+10;                                 % Shear modulus [Pa]
vxy = 0.3;                                      % Poissons ratio [-]
vyx = 0.3;                                      % Poissons ratio [-]
ny = ro*g;                                      % Specific weight[kg/m^3]

Dx = (Ex*h^3)/(12*(1-vxy*vyx));                 % Flexural rigidity [Pa*m^3]
Dy = (Ey*h^3)/(12*(1-vxy*vyx));                 % Flexural rigidity [Pa*m^3]
D1 = (Ex*vyx*h^3)/(12*(1-vxy*vyx));             % Flexural rigidity [Pa*m^3]
Dxy = (Gxy*h^3)/12;                             % Flexural rigidity [Pa*m^3

R12 = 1;
R22 = 1;
p1 = (4*Dx*pi^2)/(a^2*h);                       % [Pa]
pcr = 240E+16;                                  % Yield stress[Pa]

c = Ex*v/a;                                     % Axial stress wave velocity
                                                % [N/m^2*s]
ksi_0 = 0.1;                                    % Initial imperfection
                                                % vs. thickness


S = ((p1^3)*g*pi^2)/((c^2)*(a^2)*ny);           % Dynamic similarity number [-]

%Defining constants used in system of equations%

A = (m.^4+2*R12*m.^2*beta.^2+R22*beta.^4)/4;
B = ((1-vxy*vyx)*(m.^4+R22*beta.^4))/8;


dx = 0.001;
X = 0:dx:2;
Y = zeros(length(X));
G = Y;
Y(1) = 0;                                        % y(0)
G(1) = 0;                                        % y'(0)
tic
for i = 2:length(X)                              % RK1 (euler)
    Y(i) = Y(i-1) + dx*G(i-1);
    G(i) = G(i-1) + dx*(-S*((A*(Y(i-1)-ksi_0))+(B*(Y(i-1)^2-ksi_0^2))*Y(i-1)-
m^2*X(i-1)*Y(i-1)));
end
tid = toc;
steprate = i/tid;
disp(['    y(x = ' num2str(2) ') = ' num2str(Y(i))]);
disp(['dy/dx(x = ' num2str(2) ') = ' num2str(G(i))]);
plot(X,Y,'r')
hold on
```

8.9 Analysis with realistic yield strength

When investigating the effect of yield strength, the following are changed in the input file:

From:

```
*Material, name=Steel

*Density
```

```
7850.,
*Elastic
 2.1e+11, 0.3
*Plastic
 2.4e+18,0.
```

To:

```
*Material, name=Steel
*Density
7850.,
*Elastic
 2.1e+11, 0.3
*Plastic
 2.4e+08,0.
```